

## BIOCHEMISTRY

# The TORC1 activates Rpd3L complex to deacetylate Ino80 and H2A.Z and repress autophagy

Xin Li<sup>1</sup>, Qianyun Mei<sup>1</sup>, Qi Yu<sup>1</sup>, Min Wang<sup>2</sup>, Fei He<sup>1</sup>, Duncheng Xiao<sup>1</sup>, Huan Liu<sup>1</sup>, Feng Ge<sup>2</sup>, Xilan Yu<sup>1\*</sup>, Shanshan Li<sup>1\*</sup>

Autophagy is a critical process to maintain homeostasis, differentiation, and development. How autophagy is tightly regulated by nutritional changes is poorly understood. Here, we identify chromatin remodeling protein Ino80 and histone variant H2A.Z as the deacetylation targets for histone deacetylase Rpd3L complex and uncover how they regulate autophagy in response to nutrient availability. Mechanistically, Rpd3L deacetylates Ino80 K929, which protects Ino80 from being degraded by autophagy. The stabilized Ino80 promotes H2A.Z eviction from autophagy-related genes, leading to their transcriptional repression. Meanwhile, Rpd3L deacetylates H2A.Z, which further blocks its deposition into chromatin to repress the transcription of autophagy-related genes. Rpd3-mediated deacetylation of Ino80 K929 and H2A.Z is enhanced by the target of rapamycin complex 1 (TORC1). Inactivation of TORC1 by nitrogen starvation or rapamycin inhibits Rpd3L, leading to induction of autophagy. Our work provides a mechanism for chromatin remodelers and histone variants in modulating autophagy in response to nutrient availability.

## INTRODUCTION

Autophagy is a conserved catabolic process that breaks down cytoplasmic components, abnormal protein aggregates, and dysfunctional organelles, which can be recycled to maintain cellular and organismal homeostasis and safeguard cell survival under starvation conditions (1). The dysfunction of autophagy is implicated in human pathologies such as cancer, neurodegeneration, muscular disorder, and aging (2). Autophagy is featured by the formation of the double-membrane structure termed the autophagosome, which subsequently fuses with the vacuole or lysosome to degrade its contents (1, 3). The basal autophagy generally occurs at a low level but is induced to high levels in response to stress stimuli, such as nutrient deprivation and pathogen infection (4).

The eukaryotic cells tightly regulate and coordinate autophagy at multiple levels, including transcriptional, posttranscriptional, translational, and posttranslational controls to ensure its proper timing of induction and magnitude (4). The target of rapamycin (Tor) signaling pathway plays a major role in regulating autophagy induction. Tor is a protein kinase that promotes cellular growth and proliferation under nutrient-rich conditions (5). Tor forms two functionally distinct protein complexes, Tor complex 1 and 2 (TORC1 and TORC2) with TORC1 being sensitive to rapamycin and inactivation of TORC1 causes induction of autophagy (6). Inactivation of TORC1 causes the nucleus translocation of the protein kinase Rim15 (7), which then phosphorylates the DNA binding factor Ume6, an integral subunit of the histone deacetylase Rpd3 large (Rpd3L) complex, leading to up-regulation of autophagy-related (ATG) genes, including *ATG8* and *ATG9* (8, 9). Rpd3 exists in three complexes, Rpd3L, Rpd3S, and Rpd3 $\mu$ , with unique functions (10). Rpd3S represses cryptic transcription within gene bodies and maintains chromatin integrity (11), while Rpd3 $\mu$  is

involved in resistance to oxidative stress (12). As Rpd3L contains sequence-specific binding factors such as Ume6 and Ash1, Rpd3L is recruited to gene promoters (13, 14). In contrast, Rpd3S is recruited to the open reading frame by RNA polymerase II (RNAPII) (15). At the promoter region, Rpd3L deacetylates histones H3 and H4 to repress gene transcription (14, 16). However, Eisenberg *et al.* (17) showed that acetyl-coenzyme A (CoA) induced acetylation of histone H3K9, 14, and 18 to repress the transcription of autophagy-related genes, i.e., *ATG7*, which makes the relationship between histone (de)acetylation and autophagy more complex. Rpd3L may deacetylate other unknown proteins to repress the transcription of autophagy-related genes.

The incorporation of histone variants into chromatin provides an important way to regulate gene transcription. The histone H2A variant H2A.Z is encoded by *HTZ1* in yeast, which is highly conserved in a wide range of organisms. H2A.Z is enriched in the gene promoter regions and H2A.Z-containing nucleosomes flank the nucleosome-depleted region at transcription start sites (TSSs) (18). H2A.Z regulates the expression of genes that respond to changes in the environment and loss of H2A.Z results in defects in response to external stress by chemicals such as hydroxyurea, caffeine, formamide, and benomyl (19, 20). The functions of H2A.Z in cells are linked to the dynamics of its deposition and eviction from chromatin, which are mediated by two highly conserved, multisubunit adenosine 5'-triphosphate (ATP)-dependent chromatin remodeling complexes, INO80 and SWR-C (21). Ino80 and Swr1 are catalytic subunits of INO80 and SWR-C, respectively (19, 22–24). INO80 catalyzes the eviction of H2A.Z from chromatin, whereas SWR-C directs the incorporation of H2A.Z into nucleosomes by a dimer exchange reaction (23, 25, 26). The N-terminal domain of yeast H2A.Z is acetylated at lysines 3, 8, 10, and 14 by the NuA4 and SAGA complexes to promote its incorporation into chromatin and regulate gene expression (27–29). Despite much progress has been made toward understanding the role of INO80, SWR-C, and H2A.Z in regulating chromatin structure

Copyright © 2023 The Authors, some rights reserved; exclusive licensee American Association for the Advancement of Science. No claim to original U.S. Government Works. Distributed under a Creative Commons Attribution NonCommercial License 4.0 (CC BY-NC).

<sup>1</sup>State Key Laboratory of Biocatalysis and Enzyme Engineering, School of Life Sciences, Hubei University, Wuhan, Hubei 430062, China. <sup>2</sup>Key Laboratory of Algal Biology, Institute of Hydrobiology, Chinese Academy of Sciences, Wuhan, Hubei 430072, China.

\*Corresponding author. Email: shl@hubu.edu.cn (S.L.); yuxilan@hubu.edu.cn (X.Y.)

and gene transcription, it is unclear whether they participate in regulation of autophagy.

Although Rpd3L complex has been reported to repress the transcription of *ATG8* and *ATG9* (8, 9), little is known about the underlying mechanism. Here, we identify chromatin remodeling protein Ino80 and histone variant H2A.Z as the deacetylation targets for Rpd3L complex. We find that Rpd3L deacetylates Ino80 K929 to stabilize Ino80 and remove H2A.Z from autophagy-related genes, providing the first evidence that the stability of chromatin remodeling protein can be regulated by acetylation/deacetylation. Rpd3L also deacetylates H2A.Z at K3, 8, 10, and 14 to further reduce its incorporation into autophagy-related genes. As a consequence of deacetylation of Ino80 K929 and H2A.Z, the transcription of autophagy-related genes is repressed and the autophagy activity is maintained at lower levels under nutrient-rich conditions. Moreover, Rpd3L-mediated deacetylation of Ino80 and H2A.Z is promoted by the TORC1 pathway, which is inactivated under nitrogen starvation to induce autophagy. Thus, our work provides a mechanism to regulate autophagy in response to nutrient availability.

## RESULTS

### Ino80 interacts with Rpd3 and negatively regulates the transcription of autophagy-related genes

By analyzing the transcriptome data for *rpd3Δ* mutant by Holstege laboratory (30), we found that Rpd3 represses the transcription of a wide range of autophagy-related (*ATG*) genes in addition to *ATG8* and *ATG9* (Fig. 1A) (8, 9). By performing the ChIP-seq (chromatin immunoprecipitation combined with high-throughput sequencing) to examine the distribution of Rpd3 genome wide, we found that Rpd3 substantially binds at autophagy-related genes that constitute the core autophagy apparatus when compared with other genes bound by Rpd3 (Fig. 1A), indicating that Rpd3 plays a broad role in transcriptional repression of autophagy.

Rpd3 has been reported to catalyze the deacetylation of histones H3/H4 to repress gene expression (14, 16). To investigate whether Rpd3 inhibits autophagy by deacetylating histones, we examined autophagy activity in the mutants of histone acetylation sites (H3K9A, H3K14A, H3K18A, H3K56A, H4K5A, H4K8A, and H4K12A) using a green fluorescent protein (GFP)–Atg8 processing assay. The principle of this assay is that upon autophagy induction, GFP–Atg8 is transported into the vacuoles, where Atg8 is degraded but the free GFP moiety is resistant to proteolysis. The ratio of free GFP/GFP–Atg8 is directly correlated with the basal autophagic flux. However, none of these histone mutants had significantly reduced the autophagy activity or decreased transcription of *ATG* genes (fig. S1, A and B), which is in agreement with the findings that acetylation of histone H3K9, 14, and 18 represses instead of activates the transcription of autophagy-related genes (17). Rpd3 has been reported to repress autophagy by catalyzing the deacetylation of Atg3 at K19 and K48 (31). Still, loss of Atg3 has no significant effect on the transcription of autophagy-related genes (fig. S1, C to E).

To characterize the potential deacetylation target(s) of Rpd3, we immunoprecipitated the FLAG-tagged Rpd3 (Rpd3-FLAG) from yeast cells and mass spectrometry analysis detected the presence of INO80 complex subunits, including Ino80, Arp8, Nhp10, Arp5, Rvb1, Rvb2, Act1, etc. (Fig. 1B). INO80 complex has been

reported to regulate the expression of metabolic genes in response to nutrient changes (32), but it is unknown about the relationship between Ino80 and autophagy. Mass spectrometry analysis of immunoprecipitated Ino80-FLAG also revealed Rpd3 as the Ino80 interactor (Fig. 1B). The interaction between the endogenous Ino80 and Rpd3 was confirmed by co-immunoprecipitation (co-IP) and reciprocal IP (Fig. 1, C and D). In contrast, Rpd3 had no physical interaction with Swr1, the catalytic subunits SWR-C (fig. S1F). Moreover, loss of Ino80 in *rpd3Δ* mutant caused severe growth defects on nutrient-rich [yeast extract peptone dextrose (YPD)] medium (fig. S1G), indicating that Ino80 and Rpd3 have genetic interactions and are functionally related. All these results prompted us to investigate whether Ino80 is involved in Rpd3-mediated transcriptional repression of autophagy.

We first assessed the effect of Ino80 on autophagy activity. The GFP–Atg8 processing assay demonstrated significantly increased autophagic flux with active vacuolar proteolysis in *ino80Δ* mutant compared to its wild-type (WT) counterpart (Fig. 1, E and F). Likewise, loss of INO80 complex subunits, Arp8, Nhp10, Taf14, Ies1, and Ies2 significantly increased autophagy activity (Fig. 1, E and F, and fig. S1H). Loss of Rvb1 and knockdown of Rvb2 had no effect on autophagy, which could be due to the fact that Rvb1 and Rvb2 are common subunits of both INO80 and SWR-C complexes. To strengthen these findings, we used a complementary assay by assessing the autophagy-dependent translocation of GFP–Atg8 to the vacuole by fluorescence microscopy. The percentage of autophagic cells that displayed vacuolar localization of GFP was significantly increased in INO80 complex mutants, including *ino80Δ*, *arp8Δ*, and *nhp10Δ* (Fig. 1G). Consistently, the transcription of *ATG* genes (*ATG1*, *ATG9*, *ATG10*, *ATG11*, *ATG14*, *ATG15*, *ATG18*, and *ATG29*) was significantly increased in these mutants (Fig. 1H). To test whether Rpd3 and Ino80 are epistatic, *RPD3* and *INO80* were deleted separately and together. Deletion of *RPD3*, *INO80* alone or their codeletion led to a similar increase of autophagy activity (Fig. 1I), suggesting that Rpd3 and Ino80 act in the same pathway to regulate basal autophagy.

### Rpd3L protects Ino80 from autophagy-mediated degradation

We observed the protein level of Ino80 was significantly reduced in *rpd3Δ* mutant (Fig. 2A). Among the known histone deacetylases in yeast including Hos1, Hos2, Hos3, Hos4, Sir2, Rpd3, and Hda1, only loss of Rpd3 reduced the intracellular protein level of Ino80 (fig. S2A). Deletion of *RPD3* had no significant effect on *INO80* mRNA level (fig. S2B). We then examined the effect of Rpd3 on Ino80 protein stability. WT and *rpd3Δ* cells were treated with cycloheximide (CHX) to block protein synthesis. The overall Ino80 protein levels were significantly lower in *rpd3Δ* mutant than those in WT (Fig. 2B). Rpd3 exists in three distinct complexes, Rpd3L, Rpd3S, and Rpd3μ, with different functions (10). To identify which Rpd3 complex(es) maintains Ino80 stability, we examined Ino80 protein levels in the deletion mutants of Rpd3L-, Rpd3S-, and Rpd3μ-specific subunits. Loss of Rpd3L-specific subunits (Ash1, Sds3, Sap30, and Ume6) reduced Ino80 protein levels (fig. S2C), indicating that Ino80 is stabilized by Rpd3L complex. In accordance with these results, loss of Rpd3L subunit Sds3 significantly increased autophagy activity (fig. S2D). Loss of Rpd3L-specific subunits (Ash1, Sds3, and Sap30) but not Rpd3S (Eaf3 and Rco1) and

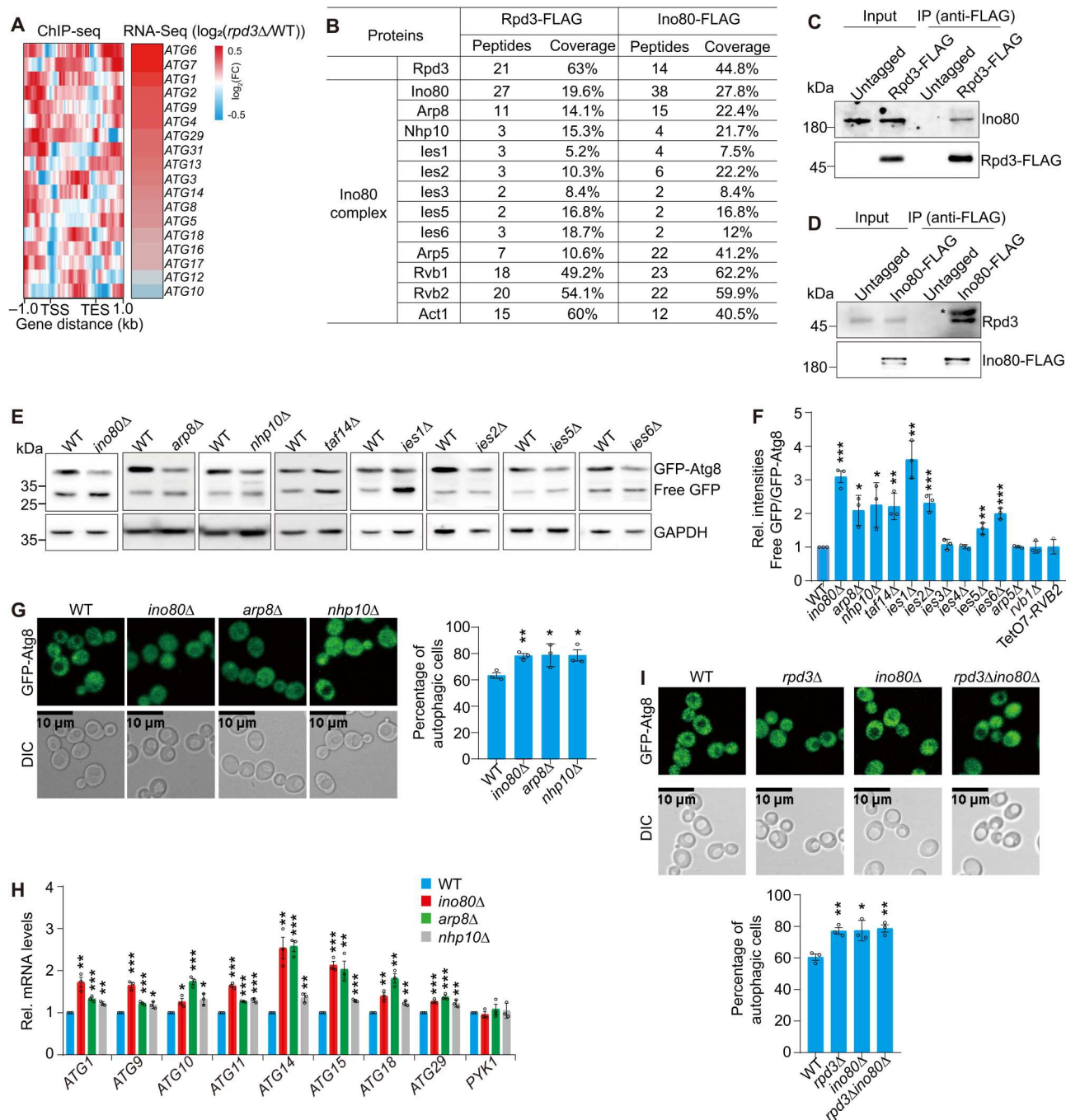


**Fig. 1. Ino80 interacts with Rpd3 and regulates autophagy.** (A) Left: Heatmap showing the occupancy of Rpd3 [ $\log_2(\text{Rpd3 IP}/\text{input})$ ] at 18 core autophagy machinery genes by ChIP-seq. Right: Heatmap showing the transcriptional changes [ $\log_2(\text{rpd3}\Delta/\text{WT})$ ] of 18 core ATG genes in *rpd3*Δ mutant by RNA-seq. (B) IP–mass spectrometry analysis of proteins copurified with Rpd3 and Ino80. The endogenously expressed Rpd3-FLAG and Ino80-FLAG were individually immunoprecipitated from cells with anti-FLAG agarose beads. (C and D) Rpd3 interacts with Ino80 as determined by co-IP assay (C) and reciprocal IP (D). The endogenously expressed Rpd3-FLAG and Ino80-FLAG were immunoprecipitated with anti-FLAG agarose beads. The untagged strain was used as a negative control. The asterisk indicates the nonspecific band. (E) Analysis of the autophagy activity in WT and INO80 complex subunit gene-null mutants as determined by the GFP-Atg8 processing assay. (F) Quantification of the immunoblot data in Fig. 1E and Fig. S1H. (G) Analysis of the autophagy activity in WT, *ino80*Δ, *arp8*Δ, and *nhp10*Δ mutants as determined by the fluorescence assay. The autophagic cells were defined as cells with clear vacuolar GFP fluorescence. (H) Analysis of the transcription of ATG genes in WT, *ino80*Δ, *arp8*Δ, and *nhp10*Δ mutants as determined by qRT-PCR. The constitutively expressed *PYK1* serves as a negative control. (I) Analysis of the autophagy activity in WT, *rpd3*Δ, *ino80*Δ, and *rpd3*Δ*ino80*Δ mutants as determined by the fluorescence assay. For (E) to (I), data represent the mean  $\pm$  SE of three biological independent experiments. \* $P < 0.05$ , \*\* $P < 0.01$ , and \*\*\* $P < 0.001$ .

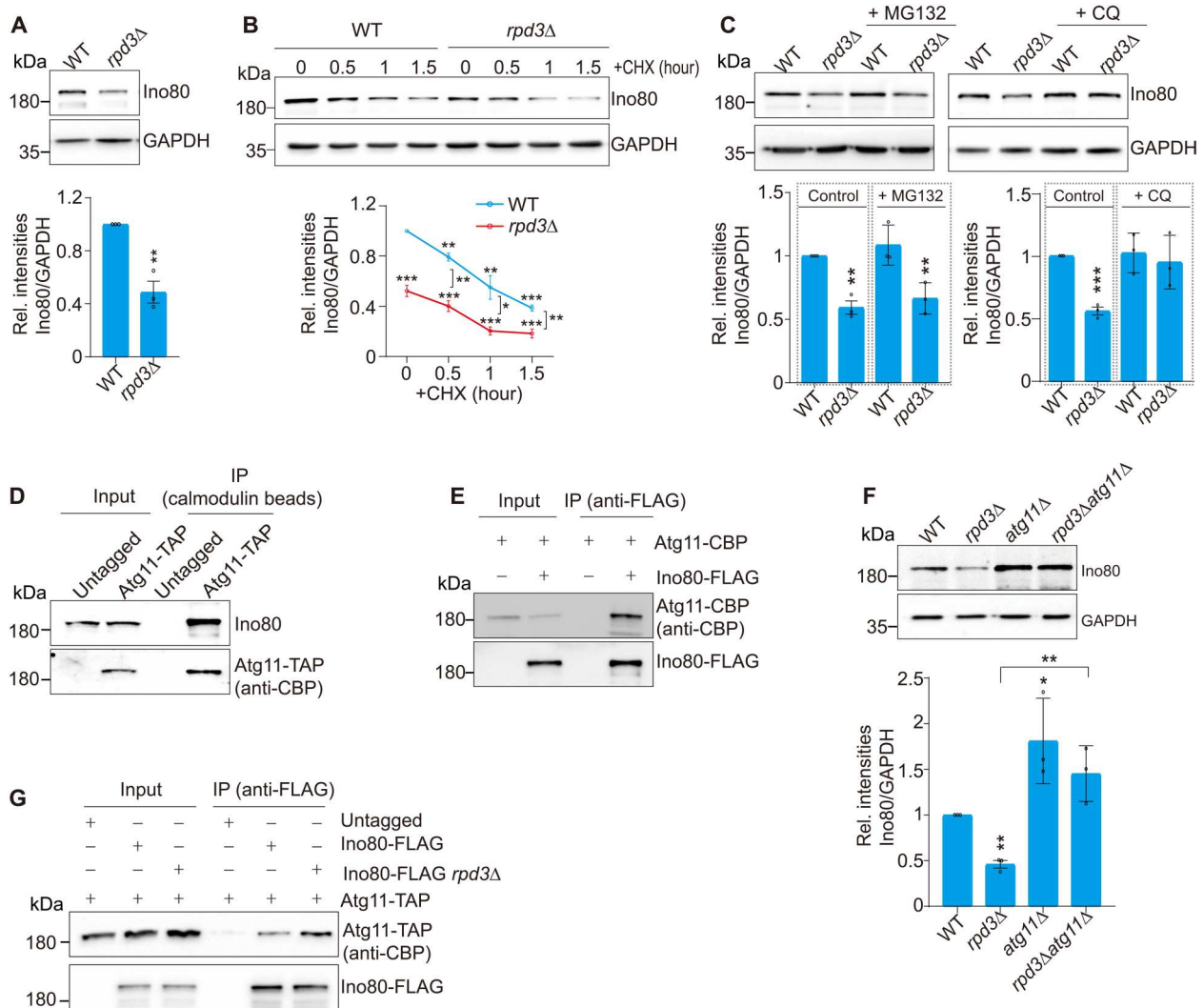


**Fig. 2. Rpd3 protects Ino80 from degrading by autophagy.** (A) Immunoblot analysis of Ino80 in WT and *rpd3Δ* mutant. GAPDH, glyceraldehyde-3-phosphate dehydrogenase. (B) Analysis of Ino80 stability in WT and *rpd3Δ* mutant. WT and *rpd3Δ* mutant were treated with CHX (0.1  $\mu$ g/ml) for 0 to 1.5 hours. (C) Analysis of the effect of MG132 and CQ on intracellular Ino80 protein levels in WT and *rpd3Δ* mutant. Cells were treated with 10  $\mu$ M MG132 or 20  $\mu$ M CQ for 2 hours. (D) Ino80 interacted with Atg11 as determined by in vivo co-IP. The endogenously expressed TAP-tagged Atg11 (Atg11-TAP) was immunoprecipitated with calmodulin beads. (E) In vitro co-IP showing that the purified Ino80-FLAG interacted with tandem affinity-purified Atg11 (Atg11-CBP). Ino80-FLAG was purified with anti-FLAG beads. The purified Ino80-FLAG was incubated with purified Atg11-CBP and immunoprecipitated with anti-FLAG beads. (F) Deletion of *ATG11* rescued the reduced Ino80 in *rpd3Δ* mutant as determined by immunoblots. (G) Loss of Rpd3 enhanced the interaction between endogenously expressed Ino80 and Atg11 as determined by co-IP assay. For (A) to (C) and (F), data represent the mean  $\pm$  SE of three biological independent experiments. \* $P$  < 0.05, \*\* $P$  < 0.01, and \*\*\* $P$  < 0.001.

Rpd3 $\mu$  (Snt2 and Ecm5) significantly increased the transcription of autophagy-related genes (fig. S2, E and F).

In eukaryotic cells, there are two major protein degradation systems to regulate protein stability: the 26S proteasome and lysosome pathways (33). To identify the mechanism(s) that degrades Ino80 in *rpd3Δ* mutant, we treated WT and *rpd3Δ* cells with the proteasome inhibitor MG132 and found that Ino80 was still reduced in *rpd3Δ* mutant after MG132 treatment (Fig. 2C). However, when cells were treated with chloroquine (CQ), an inhibitor for lysosomal proteases, the reduced Ino80 in *rpd3Δ* mutant was restored (Fig. 2C), suggesting that loss of Rpd3 accelerates autophagy-mediated degradation of Ino80.

By analyzing the mass spectrometry data for Ino80 interaction proteins, we found that Ino80 may interact with several autophagy-related proteins, including Atg2, Atg9, Atg11, Atg20, etc. (fig. S2G). The interaction between Ino80 and Atg11 was confirmed by in vivo co-IP assay and in vitro IP assays (Fig. 2, D and E). The protein level of Ino80 was significantly increased in the deletion mutants of core autophagy-related genes, especially in the deletion mutant of *ATG3*, *ATG10*, *ATG11*, and *ATG12* (fig. S2H). We thus deleted *ATG11* in *rpd3Δ* mutant and found that loss of Atg11 restored the reduced Ino80 in *rpd3Δ* mutant (Fig. 2F). Moreover, loss of Rpd3 enhanced the interaction between Ino80 and Atg11 (Fig. 2G), which may accelerate autophagy-mediated Ino80

degradation. Collectively, these data indicate that Rpd3L complex protects Ino80 from autophagy-mediated degradation.

### Rpd3L deacetylates Ino80 K929 to enhance its protein stability and transcriptionally repress autophagy

The above data showed that Rpd3L interacts with Ino80 and protects it from being degraded by autophagy. As protein acetylation has been implicated in promoting protein degradation by autophagy (34), we wondered whether Rpd3L stabilizes Ino80 by catalyzing the deacetylation of Ino80. To test this hypothesis, we immunoprecipitated Ino80 from WT and *rpd3Δ* mutant. Using the pan-acetyllysine antibody, we detected Ino80 acetylation and this acetylation was increased in *rpd3Δ* mutant (Fig. 3A). Moreover, the increased Ino80 acetylation was observed in the mutants of Rpd3L subunits, *sds3Δ* and *ume6Δ* (fig. S3A). We also purified INO80 complex from WT and *rpd3Δ* mutant and found that the catalytic subunit Ino80 was the major protein that was deacetylated by Rpd3 (Fig. 3B). By bioinformatic analysis, we identified five potential acetylation sites on Ino80, including K9, K456, K618, K929, and K1439. We individually mutated each lysine residue to arginine and found that mutation of Ino80-K929R markedly increased Ino80 protein level (Fig. 3C). When WT and Ino80-K929R mutant were treated with CHX, the Ino80 protein levels were significantly higher in Ino80-K929R mutant than WT (fig. S3B), implying that either Ino80-K929 or Ino80-K929 acetylation (Ino80 K929ac) regulates Ino80 stability.

By analyzing the acetylome profiling data by Downey *et al.* (35), we identified the peptide corresponding to Ino80 K929ac (LHMIL-KacPFMLR). Moreover, Ino80 K929 is highly conserved from yeast to mammals (fig. S3C). We thus generated the antibody that specifically recognizes acetylated Ino80 K929 (anti-Ino80 K929ac) (fig. S3D). Using the anti-Ino80 K929ac antibody, we detected the intracellular Ino80 K929ac in WT but not Ino80-K929R mutant (Fig. 3D). Deletion of *RPD3* increased Ino80 K929ac in WT but not in Ino80-K929R mutant (Fig. 3E and fig. S3E). Deletion of Rpd3L-specific subunits, *ASH1* and *SDS3*, but not Rpd3S- and Rpd3μ-specific subunits increased Ino80-K929ac (fig. S3E). To confirm that Rpd3 can directly deacetylate Ino80 K929, we performed the *in vitro* deacetylation assay with purified Rpd3 complex and Ino80. The purified Rpd3 complex reduced Ino80 K929ac in a time-dependent manner (Fig. 3F), indicating that Rpd3 can directly deacetylate Ino80 K929.

We next examined the effect of Ino80 K929ac on Ino80 protein stability. Although loss of Ino80 K929ac in Ino80-K929R mutant had no effect on *INO80* mRNA level (fig. S3F), mutation of Ino80-K929R significantly increased Ino80 protein level and rescued the reduced Ino80 in *rpd3Δ* mutant (Fig. 3G), indicating that Rpd3 deacetylates Ino80 K929 to increase its stability.

We also screened for the histone acetyltransferase (HAT) that specifically acetylates Ino80 K929. As Ino80 K929ac reduces Ino80 protein level, we examined Ino80 protein levels in the mutants of known HATs, including Gcn5, Sas2, Sas3, Rtt109, and Esa1. Deletion of *SAS3* significantly increased Ino80 protein level (fig. S3, G and H). The intracellular Ino80 K929ac was reduced in *sas3Δ* mutant (Fig. 3H). Loss of Sas3 did not further increase Ino80 protein level in Ino80-K929R mutant (Fig. 3I), indicating that Sas3 acetylates Ino80 to reduce its protein stability.

To understand how Ino80 K929ac destabilizes Ino80, we examined whether Ino80 K929ac affects the interaction between Ino80

and autophagy-related proteins. Ino80 was purified from Ino80-FLAG and Ino80-K929R-FLAG cells and then incubated with tandem affinity-purified Atg11 (Atg11-CBP). After IP with anti-FLAG agarose, less Atg11 was coimmunoprecipitated with Ino80-K929R-FLAG when compared with Ino80-FLAG (Fig. 3J). Loss of Sas3 also reduced the interaction between Ino80 and Atg11 (Fig. 3K). As loss of Rpd3 enhanced the interaction between Ino80 and Atg11 (Fig. 2G), our data indicate that Ino80 K929ac is dynamically controlled by Sas3 and Rpd3 to regulate its interaction with autophagy-related proteins.

With the increased Ino80 protein levels in Ino80-K929R mutant, the autophagy activity was significantly reduced in Ino80-K929R mutant (Fig. 3, L and M). Loss of Ino80 K929ac in Ino80-K929R mutant significantly reduced the transcription of autophagy-related genes, including *ATG1*, *ATG9*, *ATG11*, *ATG14*, *ATG15*, *ATG18*, and *ATG29* (Fig. 3N), suggesting that Ino80 K929ac reduces Ino80 protein levels to increase the transcription of *ATG* genes. Loss of Rpd3 significantly increased the transcription of *ATG* genes, while mutation of Ino80-K929R reduced the increased transcription of *ATG* genes in *rpd3Δ* mutant (Fig. 3N), consistent with the trend of Ino80 changes (Fig. 3G). Collectively, these data demonstrate that Ino80 K929 is acetylated by Sas3 and deacetylated by Rpd3L to affect its stability and transcriptionally regulate autophagy.

### Ino80 evicts H2A.Z from autophagy-related gene promoters and transcriptionally represses autophagy

The INO80 complex promotes the eviction of H2A.Z from gene promoters (25). Loss of H2A.Z leads to misregulation of genes in response to environmental and developmental stimuli (36). Analysis of H2A.Z ChIP-seq data revealed the significant enrichment of H2A.Z at the TSS of core *ATG* genes (Fig. 4A). By analyzing the RNA sequencing (RNA-seq) data for H2A.Z transcriptome (37), we revealed that a large number of autophagy-related genes were significantly down-regulated in *htz1Δ* mutant (Fig. 4A and fig. S4A). Loss of Ino80 significantly increased H2A.Z occupancy at *ATG* gene promoters (Fig. 4B). The H2A.Z occupancy at *ATG* gene promoters was significantly reduced in Ino80-K929R mutant (fig. S4B), consistent with the increased Ino80 proteins in Ino80-K929R mutant. Although loss of Rpd3 had no significant effect on H2A.Z expression, the occupancy of H2A.Z at *ATG* gene promoters was significantly increased in *rpd3Δ* mutant (fig. S4, C and D). The occupancy of H2A.Z at *ATG* gene promoters was also significantly increased in Rpd3L mutants, *ash1Δ* and *sds3Δ* (fig. S4E). Moreover, loss of *RPD3* in *htz1Δ* (*HTZ1* encodes H2A.Z) mutant caused severe growth defects (fig. S4F), suggesting that Rpd3 and H2A.Z are functional related. Mutation of Ino80-K929R significantly reduced the increased occupancy of H2A.Z at *ATG* gene promoters in *rpd3Δ* mutant (Fig. 4C), indicating that Rpd3 reduces H2A.Z occupancy in part by deacetylating Ino80 K929.

We next examined the effect of H2A.Z on autophagy-related gene transcription. The transcription of autophagy-related genes, including *ATG1*, *ATG9*, *ATG11*, *ATG14*, *ATG15*, *ATG18*, and *ATG29* was significantly down-regulated in *htz1Δ* mutant (Fig. 4D), suggesting that H2A.Z promotes autophagy at the transcriptional level. Notably, loss of H2A.Z significantly reduced the transcription of *ATG* genes in *rpd3Δ* mutant (Fig. 4D). Accordingly, loss of H2A.Z significantly reduced the basal autophagy activity

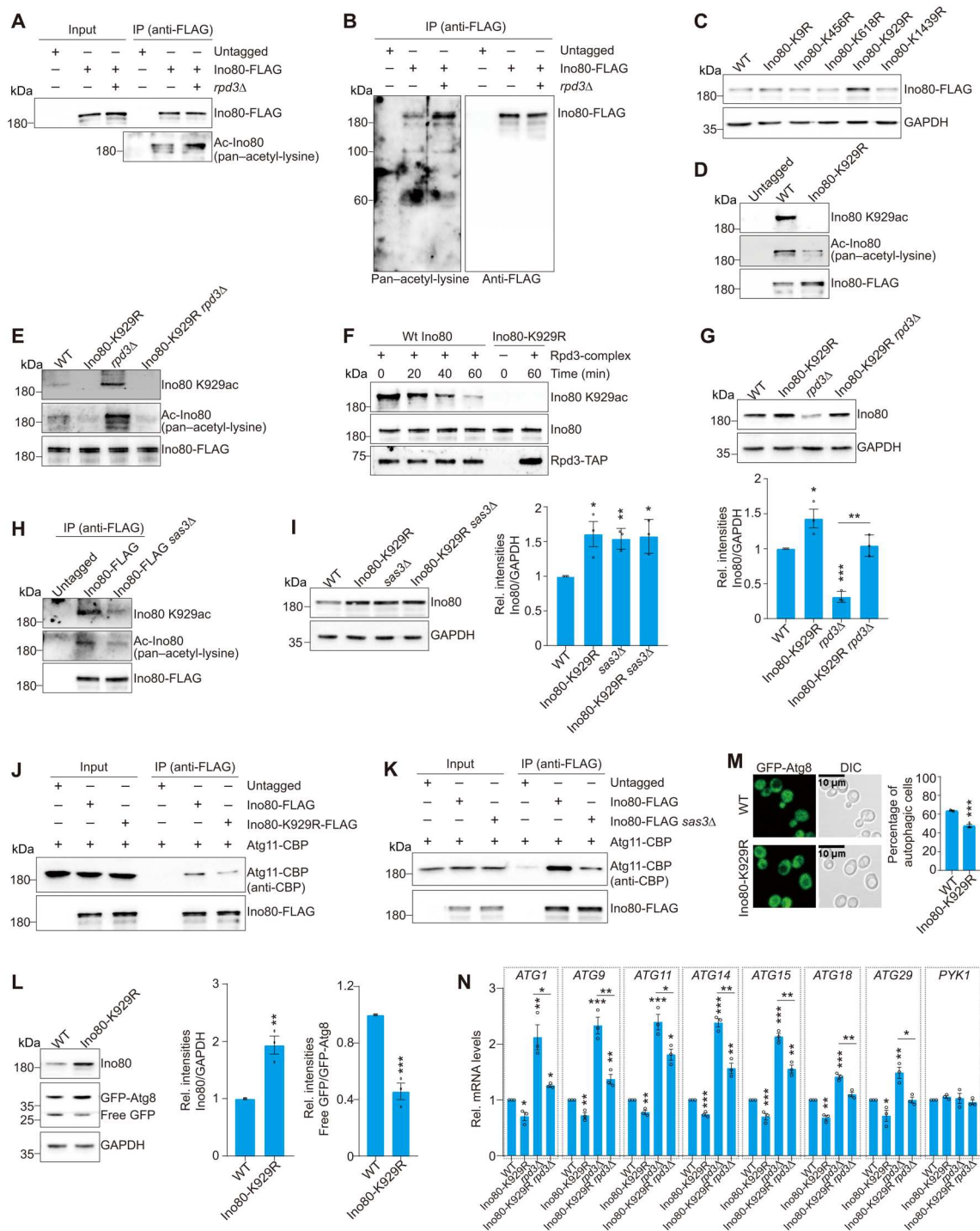


**Fig. 3. Rpd3 deacetylates Ino80 to regulate its stability and autophagy.** (A) Rpd3 deacetylates Ino80 as determined by immunoblots. The endogenously expressed FLAG-tagged Ino80 (Ino80-FLAG) was immunoprecipitated from untagged Ino80, Ino80-FLAG, and Ino80-FLAG *rpd3*Δ cells with anti-FLAG beads. Ino80 acetylation was determined by immunoblots with a pan-acetyl-lysine antibody. (B) Ino80 is the major subunit deacetylated by Rpd3 within the purified INO80 complex. (C) Immunoblot analysis of Ino80 protein levels in WT, Ino80-K9R, Ino80-K456R, Ino80-K618R, Ino80-K929R, and Ino80-K1439R mutants. (D) Ino80 is acetylated at K929. (E) Rpd3 deacetylates Ino80 at lysine-929 in vivo. (F) Rpd3 deacetylates Ino80 at lysine-929 in vitro. Equal amount of the purified WT Ino80 and Ino80-K929R was incubated with 20 ng of purified Rpd3 complex at 30°C for 0 to 60 min. (G) Immunoblot analysis of Ino80 protein levels in WT, Ino80-K929R, *rpd3*Δ, and Ino80-K929R *rpd3*Δ mutants. (H) Sas3 acetylates Ino80 at lysine-929 in vivo. (I) Immunoblot analysis of Ino80 protein levels in WT, Ino80-K929R, *sas3*Δ, and Ino80-K929R *sas3*Δ mutants. (J and K) In vitro co-IP showing loss of Ino80 K929 acetylation in Ino80-K929R mutant (J) or deletion of SAS3 (K) reduced the interaction between Ino80 and Atg11. (L and M) Effect of Ino80-K929R mutation on autophagy activity as determined by the GFP-Atg8 processing assay (L) and fluorescence assay (M). (N) Analysis of the transcription of ATG genes in WT, Ino80-K929R, *rpd3*Δ, and Ino80-K929R *rpd3*Δ mutants by qRT-PCR. For (G), (I), and (L) to (N), data represent the mean ± SE of three biological independent experiments. \**P* < 0.05, \*\**P* < 0.01, and \*\*\**P* < 0.001.

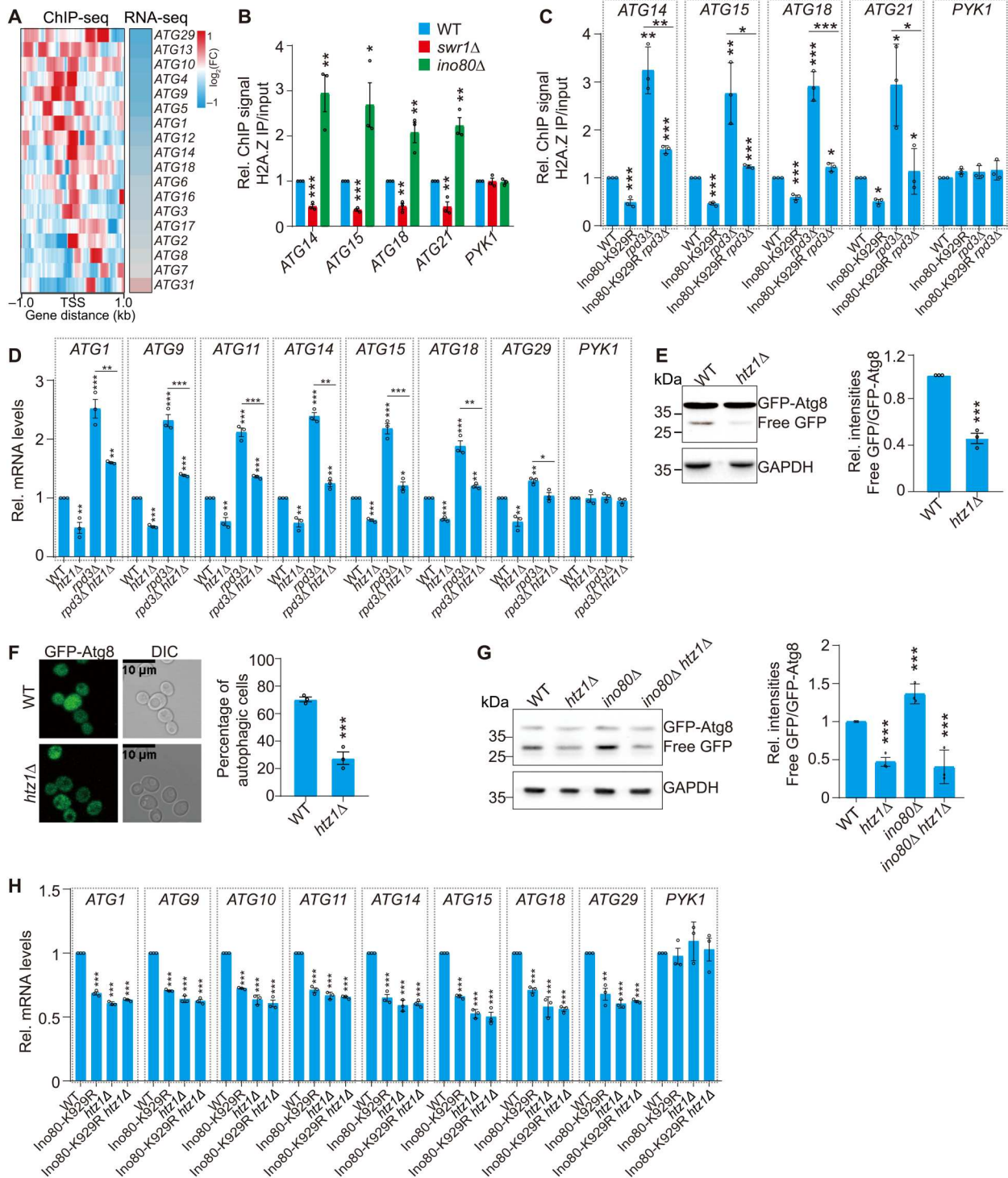


**Fig. 4. Rpd3 deacetylates Ino80 to regulate the occupancy of H2A.Z at autophagy-related genes.** (A) Left: Heatmap showing the occupancy of H2A.Z [ $\log_2(\text{H2A.Z IP}/\text{input})$ ] at 18 core autophagy machinery genes by ChIP-seq. Right: Heatmap showing the transcriptional changes [ $\log_2(\text{htz1}\Delta/\text{WT})$ ] of 18 core ATG genes in *htz1* $\Delta$  mutant by RNA-seq. (B) ChIP-qPCR analysis of H2A.Z occupancy at ATG gene promoters in WT, *swr1* $\Delta$ , and *ino80* $\Delta$  mutants when cells were grown in YPD medium. PYK1 serves as a negative control. (C) ChIP-qPCR analysis of H2A.Z occupancy at ATG gene promoters in WT, *Ino80-K929R*, *rpd3* $\Delta$ , and *Ino80-K929R rpd3* $\Delta$  mutants. (D) qRT-PCR analysis of the transcription of ATG genes in WT, *htz1* $\Delta$ , *rpd3* $\Delta$ , and *rpd3* $\Delta$  *htz1* $\Delta$  mutants when grown in YPD medium. (E and F) Effect of HTZ1 deletion on autophagy activity as determined by the GFP-Atg8 processing assay (E) and fluorescence assay (F). (G) Analysis of autophagy activity in WT, *htz1* $\Delta$ , *ino80* $\Delta$ , and *ino80* $\Delta$  *htz1* $\Delta$  mutants as determined by the GFP-Atg8 processing assay. (H) qRT-PCR analysis of the transcription of ATG genes in WT, *Ino80-K929R*, *htz1* $\Delta$ , and *Ino80-K929R htz1* $\Delta$  mutants. For (B) to (H), data represent the mean  $\pm$  SE of three biological independent experiments. \* $P < 0.05$ , \*\* $P < 0.01$ , and \*\*\* $P < 0.001$ .

(Fig. 4, E and F). These data suggest that Rpd3 reduces the incorporation of H2A.Z into the promoters of autophagy-related genes to repress their transcription.

H2A.Z is deposited into chromatin by the SWR1 complex (SWR-C) (19, 22, 23). Loss of Swr1, the catalytic subunit of SWR-C, significantly reduced H2A.Z occupancy at ATG gene promoters (Fig. 4B). By analyzing the RNA-seq data for SWR-C mutants (38), we found that ATG genes were significantly down-regulated in SWR-C mutants (fig. S4G). By quantitative reverse transcription polymerase chain reaction (qRT-PCR), we confirmed the reduced transcription of ATG genes in SWR-C mutants (*swr1Δ* and *swc2Δ*) (fig. S4H). The autophagy activity was also significantly reduced in SWR-C mutants (fig. S4, I and J). Loss of Swr1 significantly reduced autophagy activity, and deletion of *SWR1* in *htz1Δ* mutant did not further reduce the autophagy activity (fig. S4K), indicating that SWR-C enhances autophagy activity by promoting the incorporation of H2A.Z into autophagy-related genes. Meanwhile, loss of Ino80 increased the autophagy activity but deletion of *HTZ1* in *ino80Δ* mutant significantly reduced the autophagy activity (Fig. 4G). Notably, mutation of Ino80-K929R significantly reduced the transcription of ATG genes and loss of H2A.Z slightly decreased the transcription of ATG genes in Ino80-K929R mutant (Fig. 4H). These data suggest that Rpd3 stabilizes Ino80 to remove H2A.Z from autophagy-related gene promoters and repress their transcription.

### Rpd3L-mediated H2A.Z deacetylation transcriptionally represses autophagy

The N-terminal domain of yeast H2A.Z is acetylated at lysines 3, 8, 10, and 14 to regulate gene transcription (27–29). Loss of H2A.Z acetylation reduces its deposition into inducible gene promoters (29). We detected the acetylation of H2A.Z (AcH2A.Z) using the pan-acetyl-lysine antibody, and this acetylation signal was abolished when K3, K8, K10, and K14 of H2A.Z were mutated to arginine (Htz1-4KR) (Fig. 5A). Loss of Rpd3 increased AcH2A.Z but not in Htz1-4KR mutant (Fig. 5B, lane 2 versus lane 3; Fig. 5C, lane 4 versus lane 5; and fig. S5A). Moreover, the acetylation of H2A.Z was increased in the deletion mutants of Rpd3L subunits (Ash1 and Sds3) but not Rpd3S subunit (Rco1) and Rpd3μ subunit (Ecm5) (fig. S5B), indicative of deacetylation of H2A.Z by Rpd3L complex. To further confirm that Rpd3 can directly deacetylate H2A.Z, we performed in vitro deacetylase assay with purified Rpd3 complex and H2A.Z from yeast cells. Our data showed that Rpd3 reduced the acetylation signal on H2A.Z (Fig. 5D, lanes 1 to 4, and fig. S5C).

We next examined the effect of H2A.Z acetylation on autophagy. Loss of H2A.Z acetylation in Htz1-4KR mutant significantly reduced the occupancy of H2A.Z at ATG gene promoters and down-regulated the transcription of ATG genes (Fig. 5, E and F). Moreover, mutation of Htz1-4KR significantly reduced the up-regulated ATG genes in *rpd3Δ* mutant (Fig. 5G), indicating that Rpd3 represses the transcription of autophagy-related genes, in part, by deacetylating H2A.Z.

We also examined the effect of H2A.Z K3, K8, K10, and K14 acetylation on autophagy activity. Both GFP-Atg8 processing assay and fluorescence assay showed that the autophagy activity was significantly reduced in Htz1-4KR mutant (Fig. 5, H and I). Moreover, mutation of Htz1-4KR significantly reduced the increased autophagy activity in *rpd3Δ* mutant (Fig. 5J), indicating

that Rpd3 partly inhibits autophagy, if not all, by deacetylating H2A.Z at K3, K8, K10, and K14. We also constructed Ino80-K929R/Htz1-4KR double mutant. qRT-PCR revealed that the transcription of ATG genes was significantly reduced in Ino80-K929R/Htz1-4KR double mutant (Fig. 5K). Compared with Ino80-K929R and Htz1-4KR single mutant, Ino80-K929R/Htz1-4KR double mutant showed a slightly but significantly additive effect on ATG transcription (Fig. 5K), suggesting that Rpd3L-mediated deacetylation of both Ino80 and H2A.Z contributes to transcriptional repression of autophagy-related genes.

### Rpd3L-mediated deacetylation of Ino80 and H2A.Z is repressed under nitrogen starvation to induce autophagy

The above data indicate that Rpd3L can deacetylate Ino80 and H2A.Z to reduce the occupancy of H2A.Z at autophagy-related genes and repress their transcription. We next investigated how Rpd3L-mediated deacetylation of Ino80 and H2A.Z was regulated under different starvation conditions. We cultured cells in nutrient-rich (YPD medium) and then switched them to glucose starvation (SD-C) or nitrogen starvation (SD-N) conditions. As glucose starvation may reduce acetyl-CoA (39), the donor for acetylation, we first examined Ino80 protein levels instead of Ino80 acetylation under starvation conditions. Ino80 protein levels remained unchanged during glucose starvation but were reduced during nitrogen starvation conditions (fig. S6A). We thus focused on examining the effect of nitrogen starvation on Rpd3-mediated deacetylation of Ino80 and H2A.Z.

Upon nitrogen starvation, the acetylation of Ino80 and H2A.Z was significantly increased and this acetylation was abolished in Ino80-K929R and Htz1-4KR mutants (Fig. 6, A and B). Both Ino80 K929ac and AcH2A.Z remain relatively high and constant in the mutants of Rpd3L-specific subunits when cells were grown in both YPD and SD-N medium (fig. S6, B and C). Upon nitrogen starvation, Ino80 protein levels were gradually reduced and this reduction was restored by inhibiting autophagy by CQ treatment, deletion of *ATG11* or mutation of Ino80-K929R (Fig. 6C and fig. S6, D and E). Upon nitrogen starvation, the protein levels of Ino80 were reduced in both WT and *rpd3Δ* mutant (Fig. 6D), which is in agreement with the changes of Ino80 K929ac. The occupancy of H2A.Z at ATG gene promoters was increased upon nitrogen starvation (Fig. 6E). Although loss of Rpd3 increased the occupancy of H2A.Z at ATG gene promoters when cells were grown in YPD, there was no significant difference for H2A.Z occupancy at ATG genes in WT and *rpd3Δ* mutant when grown in SD-N (Fig. 6E). Moreover, the occupancy of H2A.Z at ATG gene promoters was not increased in *rpd3Δ* mutant when cells were shifted from YPD to SD-N (Fig. 6E). In line with these observations, the transcription of ATG genes was significantly induced in WT, and no significant difference was observed between WT and *rpd3Δ* mutant upon nitrogen starvation (Fig. 6F). Loss of Rpd3 did not further increase the transcription of ATG genes when cells were shifted from YPD to SD-N (Fig. 6F). Similar results were observed in Rpd3L mutants (*ash1Δ* and *sds3Δ*) (Fig. 6, E and F), indicating that loss of Rpd3L makes the expression of ATG genes less sensitive to nitrogen starvation.

The less sensitivity of *rpd3Δ* mutant to nitrogen starvation prompted us to investigate whether nitrogen starvation repressed Rpd3 activity. We purified Rpd3 complex from cells that were grown under YPD and SD-N conditions, respectively. By silver



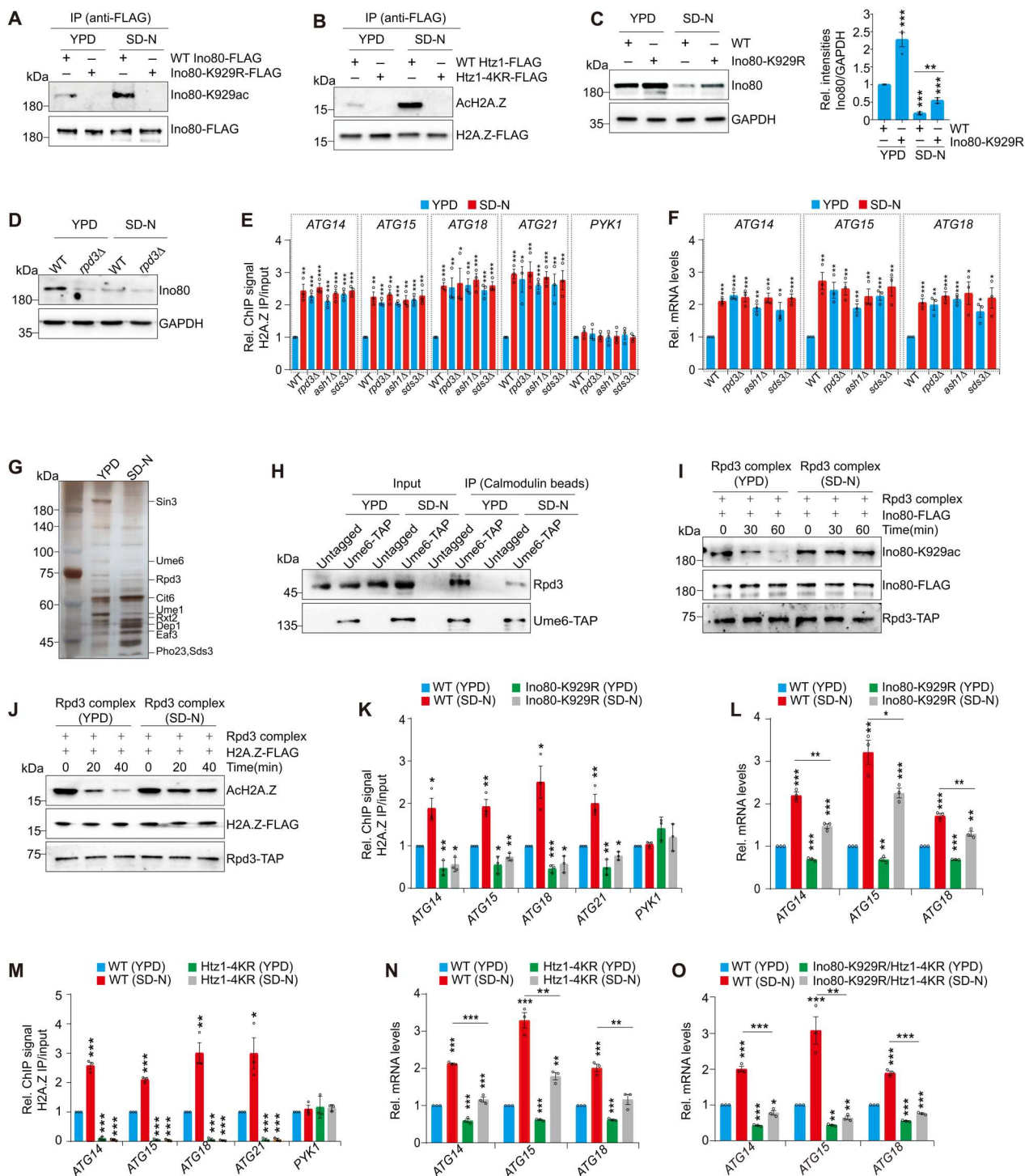


**Fig. 6. Rpd3-mediated deacetylation of Ino80 and H2A.Z is repressed to induce autophagy under nitrogen starvation.** (A) Analysis of nitrogen starvation on Ino80 K929ac. (B) Analysis of nitrogen starvation on H2A.Z acetylation. (C and D) Immunoblot analysis of Ino80 protein levels in WT, Ino80-K929R, and *rpd3Δ* mutants when grown in YPD or SD-N medium. (E) ChIP-qPCR analysis of H2A.Z occupancy at *ATG* gene promoters in WT and Rpd3L mutants (*rpd3Δ*, *ash1Δ*, and *sds3Δ*) when grown in YPD or SD-N medium. (F) qRT-PCR analysis of *ATG* transcription in WT and Rpd3L mutants (*rpd3Δ*, *ash1Δ*, and *sds3Δ*) when grown in YPD or SD-N medium. (G) Silver staining of Rpd3 complex purified from cells (Rpd3-TAP) grown in YPD or SD-N medium. (H) The interaction between Rpd3 and Ume6 was reduced when cells were grown in SD-N medium. (I and J) Nitrogen starvation reduces the activity of Rpd3 complex to deacetylate Ino80 (I) and H2A.Z (J). (K) ChIP-qPCR analysis of H2A.Z occupancy at *ATG* gene promoters in WT and Ino80-K929R mutant when grown in YPD or SD-N medium. (L) qRT-PCR analysis of *ATG* transcription in WT and Ino80-K929R mutant when grown in YPD or SD-N medium. (M) ChIP-qPCR analysis of H2A.Z occupancy at *ATG* gene promoters in WT and Htz1-4KR mutant when grown in YPD or SD-N medium. (N and O) qRT-PCR analysis of *ATG* transcription in WT, Htz1-4KR, and Ino80-K929R/Htz1-4KR mutants when grown in YPD or SD-N medium. For (C), (E), (F), and (K) to (O), data represent the mean  $\pm$  SE of three biological independent experiments. \* $P < 0.05$ , \*\* $P < 0.01$ , and \*\*\* $P < 0.001$ .

staining, we noticed that some subunits, i.e., Sin3 and Ume6, were dissociated from Rpd3 complex when cells were cultured under nitrogen starvation conditions (Fig. 6G). By co-IP, we confirmed that the interaction between endogenous Rpd3 and Ume6 was reduced upon nitrogen starvation (Fig. 6H). By performing the *in vitro* deacetylation assay, we found that the Rpd3 complex purified from cells grown in SD-N medium displayed lower activity to deacetylate Ino80 and H2A.Z when compared with Rpd3 complex purified from cells grown in YPD medium (Fig. 6, I and J). Similar to Rpd3, loss of Ume6 reduced Ino80 protein levels, increased H2A.Z occupancy at *ATG* gene promoters, and up-regulated *ATG* gene transcription when grown in YPD (fig. S6, F to H). The occupancy of H2A.Z at *ATG* genes and the transcription of *ATG* genes in *ume6* $\Delta$  mutant were less sensitive to nitrogen starvation when compared with WT (fig. S6, G and H). These data suggest that when cells were grown under nitrogen starvation conditions, the activity of Rpd3L complex is reduced, leading to increased acetylation of Ino80 and H2A.Z.

When cells were grown under nitrogen starvation conditions, the binding of Rpd3 and Ino80 at *ATG* genes was significantly reduced, whereas the binding of H2A.Z at *ATG* genes was significantly increased (fig. S6I). Although nitrogen starvation increased H2A.Z occupancy at *ATG* gene promoters in WT, the occupancy of H2A.Z at *ATG* gene promoters was significantly reduced in Ino80-K929R mutant (Fig. 6K). Accordingly, the transcription of *ATG* genes was significantly lower in Ino80-K929R mutant than WT under nitrogen starvation conditions (Fig. 6L). Similar results were observed in Htz1-4KR mutant (Fig. 6, M and N). The nitrogen starvation-induced transcription of *ATG* genes was also significantly reduced in Ino80-K929R/Htz1-4KR double mutant (Fig. 6O). The autophagy activity was significantly reduced in Ino80-K929R and Htz1-4KR mutants during nitrogen starvation conditions (fig. S6J). Collectively, these data suggest that Rpd3L deacetylates Ino80 and H2A.Z to maintain basal autophagy activity at relatively low levels; however, upon nitrogen starvation, Rpd3-mediated deacetylation of Ino80 and H2A.Z is repressed to induce autophagy to relatively high levels.

### TORC1 promotes Rpd3L-mediated deacetylation of Ino80 and H2A.Z to inhibit autophagy

The rapamycin-sensitive TORC1 has been considered to be the primary sensor of nitrogen to negatively regulate autophagy (40, 41). We hence examined whether the TORC1 pathway regulates Rpd3-mediated deacetylation of Ino80 and H2A.Z. To test this, we used rapamycin, which efficiently inhibits TORC1, and then assessed the acetylation of Ino80 and H2A.Z. After rapamycin treatment, the acetylation of both Ino80 and H2A.Z was increased in WT cells and this acetylation was lost in Ino80-K929R and Htz1-4KR mutants (Fig. 7, A and B). Along with the increased Ino80 K929ac, Ino80 protein levels were significantly reduced in WT cells but restored in Ino80-K929R mutant following rapamycin treatment (Fig. 7C and fig. S7A). Deletion of *ATG11* attenuated autophagy-induced Ino80 degradation under rapamycin treatment (fig. S7B). While WT cells had increased occupancy of H2A.Z at *ATG* genes following rapamycin treatment, the Ino80-K929R and Htz1-4KR mutants had reduced H2A.Z occupancy at *ATG* genes (Fig. 7, D and E). Mutation of Ino80-K929R or Htz1-4KR significantly reduced the rapamycin-induced transcription of *ATG* genes in WT (Fig. 7, F and G). The rapamycin-induced transcription of

*ATG* genes was also reduced in the Ino80-K929R/Htz1-4KR double mutant (fig. S7C). As a consequence, rapamycin-induced autophagy was significantly reduced in the Ino80-K929R and Htz1-4KR mutants (Fig. 7H), indicating that TORC1 inactivation increases the acetylation of Ino80-K929 and H2A.Z to promote H2A.Z incorporation at *ATG* gene promoters, which eventually up-regulates the transcription of autophagy-related genes and induces autophagy.

We then examined the effect of TORC1 inactivation on Rpd3L complex activity. Upon rapamycin treatment, the acetylation of Ino80 and H2A.Z was increased and the Ino80 protein levels were reduced in WT; loss of Rpd3L-specific subunits (Ash1 and Sds3) did not further affect Ino80 K929ac, AcH2A.Z, and the Ino80 protein levels (Fig. 7I and fig. S7D). The occupancy of H2A.Z at *ATG* genes and the transcription of *ATG* genes were high and constant in Rpd3L-specific mutants irrespective of rapamycin treatment (Fig. 7, J and K). In accordance with *ATG* gene transcription, the autophagy activity was high and constant in *rap3* $\Delta$  mutant irrespective of rapamycin treatment (fig. S7E). Rapamycin treatment also reduced the interaction between Rpd3 and another Rpd3L subunit, Ume6 (Fig. 7L), which is similar to the situation under nitrogen starvation conditions (Fig. 6, G and H). Like the *rap3* $\Delta$  mutant, the *ume6* $\Delta$  mutant had low and constant Ino80 protein levels, high and constant H2A.Z occupancy at *ATG* genes and *ATG* gene transcription regardless of rapamycin treatment (Fig. 7, M and N, and fig. S7, F and G), suggesting that Rpd3L-mediated deacetylation of Ino80 and H2A.Z is repressed after TORC1 inactivation.

One target of TORC1 is Rim15, which connects TORC1 and Rpd3L (7). Inactivation of TORC1 by rapamycin causes the nucleus translocation and activation of Rim15 (7). Active Rim15 then phosphorylates the Ume6 subunit of Rpd3L complex, which disrupts the association of Sin3 and Rpd3 and relieves transcription repression of the target genes (8, 42). To determine whether TORC1-mediated Rpd3 activation requires its downstream target, Rim15, we investigated whether loss of Rim15 affects Ino80 K929ac and AcH2A.Z. The acetylation of Ino80 and H2A.Z was reduced in *rim15* $\Delta$  mutant (fig. S7H). The Ino80 protein level was significantly increased in *rim15* $\Delta$  mutant (fig. S7I). The rapamycin-induced occupancy of H2A.Z at *ATG* genes was significantly reduced in *rim15* $\Delta$  mutant (fig. S7J). Loss of Rim15 also significantly reduced the rapamycin-induced transcription of *ATG* genes (fig. S7K).

Together, our study provides a mechanism by which TORC1 activates Rpd3L complex to deacetylate Ino80 and H2A.Z and regulate autophagy (fig. S8). When cells are grown under nutrient-rich conditions, TORC1 is activated to phosphorylate and inactivate Rim15. Rpd3L complex deacetylates Ino80 K929 to stabilize Ino80, which then removes H2A.Z from autophagy-related gene promoters. Rpd3L complex is also recruited by its associated factors like Ume6 to autophagy-related gene promoters (8), where it deacetylates H2A.Z to further reduce its incorporation into autophagy-related gene promoters, leading to their transcriptional repression. When cells are grown under nitrogen starvation conditions, TORC1 is inactivated and Rim15 translocates into the nucleus, where it phosphorylates Ume6, leading to disassembly of Rpd3L complex and its reduced activity. The acetylated Ino80 is degraded by autophagy and the acetylated H2A.Z is deposited into the

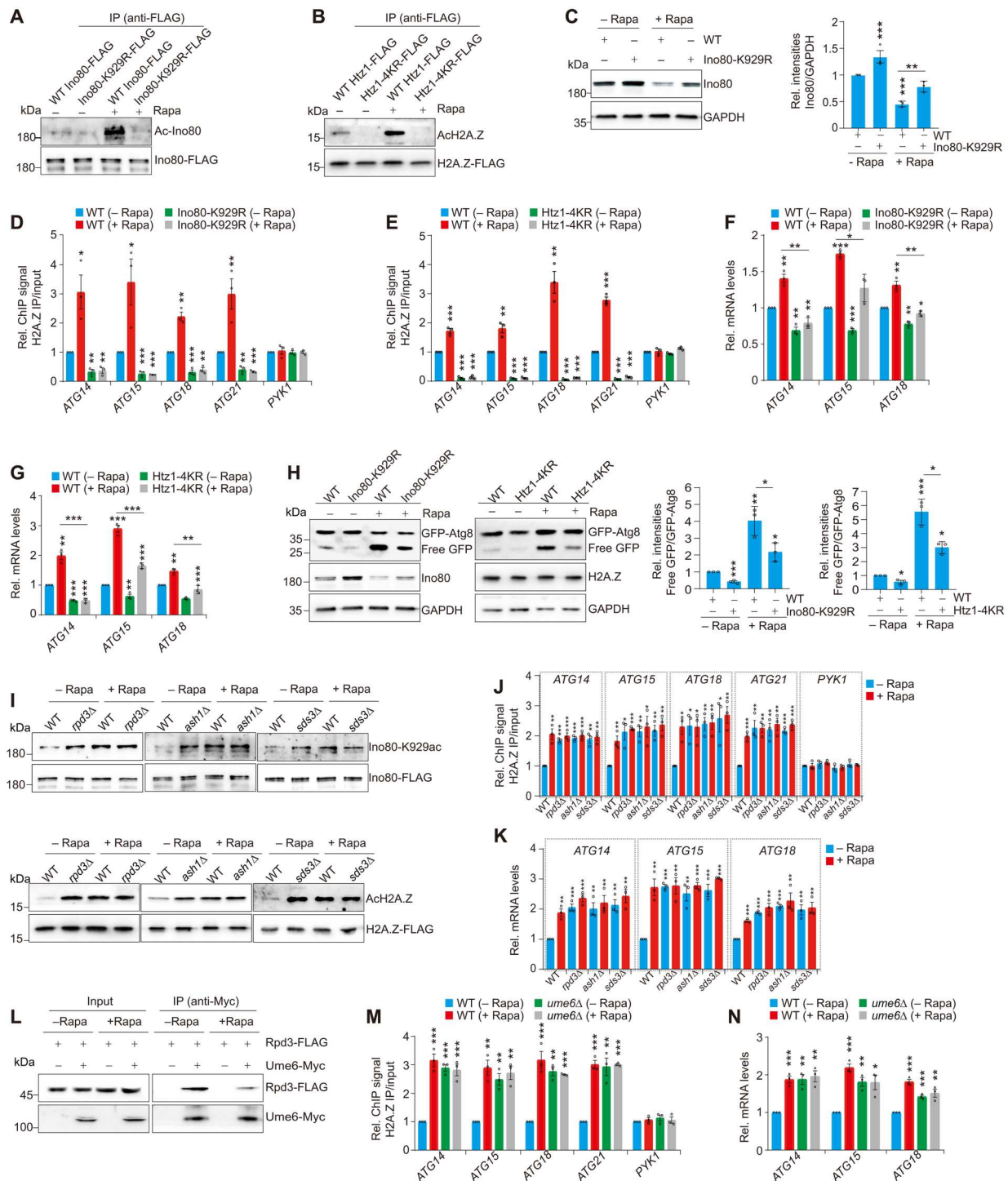


**Fig. 7. The TORC1 activates Rpd3 to deacetylate Ino80 and H2A.Z and repress autophagy.** (A and B) Immunoblot analysis of Ac-Ino80 (A) and ACh2A.Z (B) in yeast cells treated with or without rapamycin. (C) Immunoblot analysis of Ino80 protein levels in WT and Ino80-K929R mutant when treated with or without rapamycin. (D and E) ChIP-qPCR analysis of H2A.Z occupancy at ATG gene promoters in WT, Ino80-K929R, and Htz1-4KR mutants when treated with or without rapamycin. (F and G) qRT-PCR analysis of ATG transcription in WT, Ino80-K929R, and Htz1-4KR mutants when treated with or without rapamycin. (H) Analysis of autophagy activity in WT, Ino80-K929R and Htz1-4KR mutants when treated with or without rapamycin. (I) Analysis of Ino80 K929ac and ACh2A.Z in WT and Rpd3L mutants (*rrp3Δ*, *ash1Δ*, and *sds3Δ*) when treated with or without rapamycin. (J) ChIP-qPCR analysis of H2A.Z occupancy at ATG gene promoters in WT and Rpd3L mutants (*rrp3Δ*, *ash1Δ*, and *sds3Δ*) when treated with or without rapamycin. (K) qRT-PCR analysis of ATG transcription in WT and Rpd3L mutants (*rrp3Δ*, *ash1Δ*, and *sds3Δ*) when treated with or without rapamycin. (L) Rapamycin reduced the interaction between endogenous Rpd3 and Ume6. (M) ChIP-qPCR analysis of H2A.Z occupancy at ATG gene promoters in WT and *ume6Δ* mutant when treated with or without rapamycin. (N) qRT-PCR analysis of ATG transcription in WT and *ume6Δ* mutant when treated with or without rapamycin. For (C) to (H), (J), (K), (M), and (N), data represent the mean ± SE of three biological independent experiments. \**P* < 0.05, \*\**P* < 0.01, and \*\*\**P* < 0.001.

autophagy-related gene promoters to enhance the transcription of autophagy-related genes, which eventually accelerates autophagy.

## DISCUSSION

Although the histone deacetylase complex Rpd3L has been reported to repress the transcription of *ATG8* and *ATG9* (8, 9), little is known about the underlying mechanism. Here, we not only found that Rpd3L complex has a broad role in transcriptionally repressing autophagy-related gene transcription but also identified Ino80 and H2A.Z as the deacetylation targets for Rpd3L. When cells are grown in nutrient-rich condition, TORC1 activates Rpd3 to deacetylate Ino80 and H2A.Z. Rpd3L deacetylates Ino80 at K929 to stabilize Ino80 and facilitate the eviction of H2A.Z from autophagy-related gene promoters. Moreover, Rpd3L deacetylates H2A.Z at K3, 8, 10, and 14 to further reduce its incorporation into chromatin. As a consequence, the transcription of autophagy-related genes is repressed and the autophagy activity is reduced, which ensures that the basal autophagy activity is low under nutrient-rich condition. When cells are grown under nitrogen starvation condition, TORC1 is inactivated and Rim15 is derepressed and translocated into the nucleus, where it phosphorylates Rpd3L subunit Ume6, leading to dissociation and inactivation of Rpd3L complex. As a consequence, Ino80 acetylation is increased and degraded by autophagy. H2A.Z acetylation is elevated and its deposition into chromatin is enhanced to induce the transcription of autophagy-related genes (fig. S8). Therefore, our work provides an epigenetic mechanism to regulate autophagy in response to environmental nutritional cues.

In this study, we observed that the autophagy activity was not reduced in some mutants of histone acetylation sites. The increased autophagy in H3K9A, H3K14A, and H3K18A mutants is consistent with the report that acetylation of histone H3K9, 14, and 18 represses instead of activates the transcription of autophagy-related genes (17). The anticorrelation between histone acetylation and autophagy has been observed for a long time. In yeast, rapamycin treatment reduces H4 acetylation (43). Spermidine treatment reduces global histone H3 acetylation by inhibiting HATs, which up-regulates the transcription of autophagy-related genes (44). There are two possible reasons to explain the up-regulated autophagy in these histone acetylation mutants. First, certain histone acetylation marks may affect chromatin assembly. For example, the acetylation of histone H4K5, K8, and K12 is involved in newly chromatin assembly (45). Mutation of H4K5A, H4K8A, and H4K12A may hinder chromatin assembly and make chromatin less compact, which then up-regulates gene transcription. Second, certain histone acetylation may recruit other factors to repress *ATG* gene transcription. For example, H4K20 acetylation could repress gene transcription by recruiting the transcription repressor, neuron-restrictive silencer factor/repressor element 1-silencing transcription (NRSE/REST) (46). Further efforts are required to address whether these histone acetylation marks directly regulate *ATG* gene transcription.

The expression of many autophagy-related genes is substantially up-regulated in response to nutrient starvation conditions. This prompt up-regulation of autophagy-related gene expression is critical for optimal autophagy efficiency and energy usage (4). However, the transcriptional regulation of autophagy-related genes is still obscure. The transcription of autophagy-related

genes has been reported to be regulated by few histone modifications. Under starvation conditions, the reduced H2B monoubiquitination (H2Bub1) results in the activation of autophagy by controlling the transcription of autophagy-related genes (47). The acetyltransferase hMOF-catalyzed H4K16ac is involved in autophagy regulation (48). The coactivator-associated arginine methyltransferase 1 (CARM1) facilitates the transcription of autophagy-related and lysosomal genes via H3K17 dimethylation (H3R17me2) (49). We have reported that pyruvate kinase Pyk1-containing serine-responsive SAM-containing metabolic enzyme (SESAME) complex represses the transcription of autophagy-related genes by phosphorylating histone H3T11 (50). Rpd3L complex has been reported to repress the transcription of *ATG8* and *ATG9* (8, 9). However, Eisenberg *et al.* (17) showed that acetyl-CoA induced the acetylation of histone H3K9, 14, and 18 to repress the transcription of autophagy-related genes, i.e., *ATG7*. We also showed that ablation some of histone H3 and H4 acetylation sites increased the transcription of autophagy-related genes (fig. S1B), which makes the relationship between histone (de)acetylation and autophagy more complicated. Here, we revealed that Rpd3L complex represses the transcription of autophagy-related genes not by deacetylating canonical histones but by deacetylating chromatin remodeling protein Ino80 and histone variant H2A.Z. By deacetylating Ino80 and H2A.Z, Rpd3 reduces the deposition of H2A.Z into chromatin and represses the transcription of autophagy-related genes. Our work thus solved the seemingly paradoxical results that both histone deacetylases and histone acetylation inhibit autophagy.

We found that histone H2A variant H2A.Z represents an important level for transcriptional regulation of autophagy. H2A.Z is preferentially enriched at the regions of transcriptional start sites (51, 52), suggesting a relationship between H2A.Z and gene transcription. However, significant arguments still exist about whether and how this histone variant is involved in transcriptional regulation. In yeast, RNAPII and TATA-binding protein (TBP) could not be efficiently recruited to *GAL1-10* promoter in cells lacking H2A.Z (53). H2A.Z enrichment at the +1 nucleosome correlates with decreased RNAPII stalling and regulates productive elongation by facilitating H2A.Z/H2B dimer loss (54, 55). Thus, H2A.Z deposition acts as an activator of gene transcription. However, H2A.Z has been reported to occupy at the repressed promoters of some inducible genes, such as *PHO5* and *ADE17* (56, 57). Our results revealed an active role of H2A.Z in transcription of autophagy-related genes and this activation is related to acetylation of H2A.Z at lysines 3, 8, 10, and 14. The acetylated H2A.Z could either facilitate SWR-C catalyzed H2A.Z incorporation or prevent INO80-mediated H2A.Z eviction (27). INO80 prefers to remove unacetylated H2A.Z but is insensitive to evict acetylated H2A.Z (25). Hence, Rpd3-mediated H2A.Z deacetylation could either promote H2A.Z eviction by INO80 or hinder H2A.Z incorporation by SWR-C. It is also possible that H2A.Z acetylation directly promotes *ATG* gene transcription.

We provide a direct connection between histone deacetylase Rpd3L and chromatin remodeling protein. We found that Rpd3 stabilizes Ino80 by deacetylating Ino80 and provided the first evidence that Ino80 protein stability is regulated by acetylation. Thus, Rpd3 reduces the occupancy of H2A.Z at chromatin in part by deacetylating Ino80 and increasing its protein stability. The mammalian Ino80 has been reported to be ubiquitinated and degraded by the proteasome pathway (58). In contrast, our data showed that the yeast Ino80 is degraded by autophagy instead of the proteasome

pathway. Moreover, Ino80 can be acetylated at K929, which then promotes its degradation by autophagy. As Ino80 K929 is highly conserved from yeast to mammals (fig. S3C), it is possible that Ino80 could also be acetylated in mammals to control its stability. Thus, we identified a mechanism to modulate the expression and activity of the chromatin remodeling protein Ino80. We noted that Ino80 K929 resides within the ATPase domain (698-1018) of Ino80. It is possible that acetylation of Ino80 K929 may affect its chromatin remodeling activity in addition to modulating its stability. Further efforts are required to answer this question.

Nucleosome dynamics associated with the incorporation/eviction of H2A.Z is one of the key chromatin remodeling mechanisms associated with environmental response (36). Ino80 has been reported to regulate the expression of metabolic genes in response to nutrient changes (32). TORC1 phosphorylates the transcription factors, Msn2/4, Dot6, and Tod6, which then regulate the transcription of ribosome biogenesis, nitrogen metabolism, and stress response (32, 59). Here, we showed that Ino80 and Rpd3L directly play a central role in TORC1 pathway, which connects chromatin remodeling and histone variants with nutrient availability. Ino80 stability and H2A.Z occupancy are highly responsive to nitrogen starvation. Nitrogen starvation induces loss of Ino80 and increased H2A.Z occupancy at autophagy-related genes, which induces the transcription of autophagy-related genes. The TORC1-promoted deacetylation of Ino80 and H2A.Z by Rpd3L links perception of the nutrients, chromatin remodeling, and transcription in the context of autophagy regulation. Thus, our study provides a direct link between metabolic states with chromatin structure changes.

Together, we identified the chromatin remodeling protein Ino80 and histone variant H2A.Z as the deacetylation targets of Rpd3L complex. Rpd3L deacetylates Ino80 and H2A.Z to transcriptionally regulate autophagy in response to nutrient availability. Therefore, our work provides not only a pathway for chromatin remodeler to communicate metabolic status to chromatin but also an epigenetic mechanism to regulate autophagy in response to environmental nutritional cues and optimize cell fitness.

## MATERIALS AND METHODS

### Yeast strains

All yeast strains used in this study were listed in table S1. The promoter-shutoff mutants (WT TetO<sub>7</sub>, TetO<sub>7</sub>-ARP4, TetO<sub>7</sub>-SWC4, and TetO<sub>7</sub>-RVB2) were purchased from Yeast Tet-promoters Hughes Collection in Open Biosystems (GE Dharmacon). The gene deletion mutants and genomic integration of C-terminal epitope tags were constructed by homologous recombination of PCR fragments. All yeast strains were verified by colony PCR, DNA sequencing, RT-qPCR, and/or immunoblots.

### Cell growth and treatment

For most experiments, yeast cells were grown in 2% glucose-containing YPD medium at 30°C until OD<sub>600</sub> (optical density at 600 nm) of 0.7. For nitrogen starvation treatment, cells were grown in YPD until OD<sub>600</sub> of 0.7 and then pelleted at 3000 rpm for 5 min. After being washed with sterile ddH<sub>2</sub>O twice, cells were grown in SD-N medium (0.17% yeast nitrogen base without amino acids and ammonium sulfate, 2% glucose) for 0 to 2 hours. For glucose starvation treatment, cells were grown in YPD until OD<sub>600</sub> of 0.7 and then pelleted at 3000 rpm for 5 min. After being washed with

sterile ddH<sub>2</sub>O twice, cells were grown in SD-C medium (0.67% yeast nitrogen base without amino acids, supplemented with amino acids, no dextrose) for 0 to 48 hours. To knock down the expression of ARP4, SWC4, and RVB2, WT TetO<sub>7</sub>, TetO<sub>7</sub>-ARP4, TetO<sub>7</sub>-SWC4, and TetO<sub>7</sub>-RVB2 mutants were grown in YPD medium until OD<sub>600</sub> of 0.5 to 0.7 and then treated with doxycycline (50 µg/ml) for 4 hours. For rapamycin treatment, cells were grown in YPD until OD<sub>600</sub> of 0.5 to 0.7. Rapamycin (2 µg/ml) was added into the medium and cells were then grown for 0 to 1 hour. For CHX treatment, cells were treated with CHX (0.1 µg/ml) for 0 to 1.5 hours. For MG132 and CQ treatment, cells were treated with 10 µM MG132 or 20 µM CQ for 2 hours.

### Immunoblot analysis

Immunoblot analysis was performed following procedures previously described in (60). In brief, cells were grown in 5 ml of YPD or indicated medium until OD<sub>600</sub> of 0.7 to 1.0. Cells were harvested, lysed in the lysis buffer (2 M NaOH and 8% 2-mercaptoethanol), and centrifuged at 13,000 rpm. The protein pellet was resuspended in 150 µl 2× SDS sample buffer. Protein samples were separated by 8 to 15% SDS-polyacrylamide gel electrophoresis (PAGE) and transferred to polyvinylidene difluoride membrane. The blots were probed by primary antibodies, followed by incubation with horseradish peroxidase-labeled immunoglobulin G (IgG) secondary antibodies. The protein bands were visualized using the ECL Chemiluminescence Detection Kit (Bio-Rad, 170-5061) and quantified with ImageJ software (v.1.8.0).

### Antibodies

Antibody against anti-histone H2A.Z (1:5000; ab4626) was purchased from Abcam; antibody against Rpd3 (1:500; sc-514160) was purchased from Santa Cruz Biotechnology; antibodies against GFP (1:5000; 66002-1-1g), Myc (1:5000; 60003-2-1g), goat polyclonal anti-mouse IgG (1:5000; SA00001-1), and goat polyclonal anti-rabbit IgG (1:5000; SA00001-2) were obtained from Proteintech; antibody against pan-acetyl-lysine (1:2000, 9441S) was purchased from Cell Signaling Technology; antibody against FLAG M2 (1:3000; F1804-1MG) was obtained from Sigma-Aldrich; antibody against CBP (1:2000; Abs130593) was purchased from Absin Bioscience Inc.; and antibodies against Ino80 (1:500) and Ino80 K929ac (1:500) were custom-made in Abclonal. The specificity of the custom-made antibodies was confirmed by immunoblot analysis with cell extract or IP of corresponding mutants (Fig. 3D and fig. S9).

### ChIP assay

ChIP assay was performed following procedures previously described in (60). Cells were grown in 200 ml of YPD media or indicated medium at 30°C until OD<sub>600</sub> of 1.0. The cross-linking was performed in 1% formaldehyde and quenched by adding 10 ml of 2.5 M glycine. Harvested cells were resuspended in FA buffer [0.1% SDS, 40 mM Hepes-KOH (pH 7.5), 1 mM EDTA (pH 8.0), 1% Triton X-100, 0.1% Na deoxycholate, 1 mM phenylmethylsulfonyl fluoride (PMSF), leupeptin (2 µg/ml), pepstatin A (1 µg/ml), protease inhibitor cocktail, and phosphatase inhibitor cocktail] and lysed with glass beads. Chromatin was sonicated to an average size of ~500 bp and immunoprecipitated with antibodies prebound to protein G Dynabeads (Invitrogen) at 4°C overnight. The beads were washed successively with FA buffer, FA buffer + 1 M NaCl,

FA buffer + 0.5 M NaCl, TEL buffer [10 mM tris (pH 8.0), 1 mM EDTA, 0.25 M LiCl, 1% NP-40, and 1% Na deoxycholate] and TE [10 mM tris (pH 7.4) and 1 mM EDTA]. The eluted DNA/protein complexes were treated with 20  $\mu$ g of proteinase K (Roche) at 55°C for 1 hour and the cross-link was reversed at 65°C overnight. RNA was removed by RNase (Roche) treatment. DNA was then purified with ethanol precipitation and quantitated by qPCR using primers listed in table S2.

For ChIP-seq, the libraries were constructed and sequenced on an Illumina platform. Reads were aligned to yeast genome sacCer3 from UCSC using bowtie2 version 2.1.0 with parameter -k 1. Data were put into R (3.1.0) for further analysis. Peaks were called using MACS2 (v.2.1.1, macs2 callpeak) with parameter -t -c -g 1.2e7 -n -B -q 0.01 --nomodel. Peak annotation was performed on a website service (<https://manticore.niehs.nih.gov/pavis2/>). Tracks were smoothed by deepTools2 (v.2.0) and visualized by IGV software (v.2.0) with a reference genome of *Saccharomyces cerevisiae* (sacCer3).

### In vitro histone deacetylase assay

Rpd3 complex was affinity purified from 2 liters of yeast cells (TAP-Rpd3) when grown in YPD or SD-N medium as described (61). H2A.Z-FLAG and Ino80-FLAG were purified from yeast cells by anti-FLAG M2 affinity gel (GenScript). The purified H2A.Z and Ino80 were then individually incubated with purified Rpd3 complex in the reaction buffer [10 mM tris-HCl (pH 8.0), 150 mM NaCl, 1 mM MgOAc, 1 mM imidazole, 2 mM EGTA (pH 8.0), 10 mM 2-mercaptoethanol, 0.1% NP40, and 10% glycerol] at 30°C. The reaction was quenched by 2 $\times$  SDS-PAGE loading buffer and boiled at 95°C for 10 min. The reaction products were analyzed by immunoblots with indicated antibodies.

### Quantitative RT-PCR

The RNA was extracted from the yeast cells of the exponential growth period by the phenol-chloroform extraction method (50). The extracted RNA was treated with RNase-free deoxyribonuclease I (Takara, 2270A) to remove DNA and quantified by Nanodrop 2000 (Thermo Fisher Scientific). The RNA quality was determined by agarose gel electrophoresis. RNA (0.5  $\mu$ g) was taken for complementary DNA (cDNA) synthesis in the NovoScriptPlus All-in-one First Strand cDNA Synthesis SuperMix (Novoprotein). The qPCR was carried out using iTaq Universal SYBR Green Supermix (Bio-Rad, 1725121). Primers used for RT-qPCR were described in table S2.  $2^{-\Delta\Delta Ct}$  was used to calculate the quantity of relative transcription level.

### Microscopy analysis

The microscopy and imaging processing were performed as described (50). Yeast cells were cultured in YPD medium until OD<sub>600</sub> of 0.7 to 1.0. After washing with cold phosphate-buffered saline (PBS) for three times, cells were suspended in 200  $\mu$ l of PBS. Cells were visualized using a ZEISS LSM710 microscope (Germany) with a 100 $\times$  oil immersion objective by fluorescent microscopy. Images were acquired using ZEN Imaging Software ZEN 2.1 (ZEISS).

### Sample preparation and mass spectrometry analysis

Yeast cells were grown in 1.2 liters of YPD media until an OD<sub>600</sub> of 1.0, washed with PBS, and flash frozen in liquid nitrogen. Thawed

cell pellets were resuspended in IP buffer [40 mM HEPES-KOH (pH 7.5), 150 mM NaCl, 10% glycerol, and 0.1% Tween-20] and lysed with glass beads using a Biospec bead beater. The lysate was centrifuged at 45,000 rpm at 4°C for 1.5 hours and the supernatant was incubated with anti-FLAG M2 affinity gel (GenScript) at 4°C for 4 hours. The beads were washed extensively in IP buffer. The immunoprecipitated proteins were digested overnight with sequencing-grade trypsin (Promega) at 37°C and the supernatant peptides were then desalted using C18 columns (Thermo Fisher Scientific) and lyophilized. The dried peptides were reconstituted in 0.1% FA and loaded onto an Acclaim PepMap 100 C18 LC column (Thermo Fisher Scientific) using a Thermo Easy nLC 1000 LC system (Thermo Fisher Scientific) connected to Q Exactive HF mass spectrometer (Thermo Fisher Scientific). The raw mass spectrometry data were searched against the *S. cerevisiae* proteome database from Uniprot (<https://uniprot.org/proteomes/UP000002311>) using Sequest HT, MS Amanda, and ptmRS algorithms in Proteome Discoverer 2.3 (Thermo Fisher Scientific).

### Coimmunoprecipitation

Yeast whole-cell extract was prepared by vortexing with glass beads. Pre-cleared cell lysate was incubated with anti-FLAG M2 agarose (GenScript) or calmodulin beads (GE Healthcare) for 1 hour at 4°C. The beads were washed three times with IP washing buffer [40 mM HEPES-KOH (pH 7.5), 0.1% Tween-20, 10% glycerol, 1 mM PMSF, 150 mM NaCl, leupeptin (2  $\mu$ g/ml), and pepstatin A (1  $\mu$ g/ml)] and boiled in SDS sample buffer for 10 min. Supernatants from the boiled beads were subjected to SDS-PAGE and immunoblots.

### Statistics and reproducibility

Statistical differences in this study were determined by two-tailed unpaired *t* test and a *P* value <0.05 was considered statistically significant. All quantitative data were presented as mean values  $\pm$  SEM from at least three biological independent experiments. \**P* < 0.05, \*\**P* < 0.01, and \*\*\**P* < 0.001.

### Supplementary Materials

This PDF file includes:

Figs. S1 to S9  
Tables S1 to S2

[View/request a protocol for this paper from Bio-protocol.](#)

### REFERENCES AND NOTES

1. N. Mizushima, D. J. Klionsky, Protein turnover via autophagy: Implications for metabolism. *Annu. Rev. Nutr.* **27**, 19–40 (2007).
2. T. Shintani, D. J. Klionsky, Autophagy in health and disease: A double-edged sword. *Science* **306**, 990–995 (2004).
3. Z. Xie, D. J. Klionsky, Autophagosome formation: Core machinery and adaptations. *Nat. Cell Biol.* **9**, 1102–1109 (2007).
4. E. Delorme-Axford, D. J. Klionsky, Transcriptional and post-transcriptional regulation of autophagy in the yeast *Saccharomyces cerevisiae*. *J. Biol. Chem.* **293**, 5396–5403 (2018).
5. M. K. Holz, B. A. Ballif, S. P. Gygi, J. Blenis, mTOR and S6K1 mediate assembly of the translation preinitiation complex through dynamic protein interchange and ordered phosphorylation events. *Cell* **123**, 569–580 (2005).
6. R. Loewith, E. Jacinto, S. Wullschlegel, A. Lorberg, J. L. Crespo, D. Bonenfant, W. Oppliger, P. Jenoe, M. N. Hall, Two TOR complexes, only one of which is rapamycin sensitive, have distinct roles in cell growth control. *Mol. Cell* **10**, 457–468 (2002).

7. I. Pedruzzi, F. Dubouloz, E. Camerini, V. Wanke, J. Roosen, J. Winderickx, C. de Virgilio, TOR and PKA signaling pathways converge on the protein kinase Rim15 to control entry into G0. *Mol. Cell* **12**, 1607–1613 (2003).
8. C. R. Bartholomew, T. Suzuki, Z. du, S. K. Backues, M. Jin, M. A. Lynch-Day, M. Umekawa, A. Kamath, M. Zhao, Z. Xie, K. Inoki, D. J. Klionsky, Ume6 transcription factor is part of a signaling cascade that regulates autophagy. *Proc. Natl. Acad. Sci. U.S.A.* **109**, 11206–11210 (2012).
9. M. Jin, D. J. Klionsky, Transcriptional regulation of ATG9 by the Pho23-Rpd3 complex modulates the frequency of autophagosome formation. *Autophagy* **10**, 1681–1682 (2014).
10. S. L. McDaniel, B. D. Strahl, Stress-free with Rpd3: A unique chromatin complex mediates the response to oxidative stress. *Mol. Cell. Biol.* **33**, 3726–3727 (2013).
11. E. J. Wagner, P. B. Carpenter, Understanding the language of Lys36 methylation at histone H3. *Nat. Rev. Mol. Cell Biol.* **13**, 115–126 (2012).
12. L. A. Baker, B. M. Ueberheide, S. Dewell, B. T. Chait, D. Zheng, C. D. Allis, The yeast Snt2 protein coordinates the transcriptional response to hydrogen peroxide-mediated oxidative stress. *Mol. Cell. Biol.* **33**, 3735–3748 (2013).
13. M. J. Carozza, L. Florens, S. K. Swanson, W. J. Shia, S. Anderson, J. Yates, M. P. Washburn, J. L. Workman, Stable incorporation of sequence specific repressors Ash1 and Ume6 into the Rpd3L complex. *Biochim. Biophys. Acta* **1731**, 77–87 (2005).
14. D. Kadosh, K. Struhl, Repression by Ume6 involves recruitment of a complex containing Sin3 corepressor and Rpd3 histone deacetylase to target promoters. *Cell* **89**, 365–371 (1997).
15. C. K. Govind, H. Qiu, D. S. Ginsburg, C. Ruan, K. Hofmeyer, C. Hu, V. Swaminathan, J. L. Workman, B. Li, A. G. Hinnebusch, Phosphorylated Pol II CTD recruits multiple HDACs, including Rpd3C(S), for methylation-dependent deacetylation of ORF nucleosomes. *Mol. Cell* **39**, 234–246 (2010).
16. D. Kadosh, K. Struhl, Targeted recruitment of the Sin3-Rpd3 histone deacetylase complex generates a highly localized domain of repressed chromatin in vivo. *Mol. Cell. Biol.* **18**, 5121–5127 (1998).
17. T. Eisenberg, S. Schroeder, A. Andryushkova, T. Pendl, V. Küttner, A. Bhukel, G. Mariño, F. Pietrocola, A. Harger, A. Zimmermann, T. Moustafa, A. Sprenger, E. Jany, S. Büttner, D. Carmona-Gutierrez, C. Ruckstuhl, J. Ring, W. Reichelt, K. Schimmel, T. Lee, C. Moser, S. Schatz, L. P. Kamolz, C. Magnes, F. Sinner, S. Sedej, K. U. Fröhlich, G. Juhasz, T. R. Pieber, J. Dengjel, S. J. Sigrist, G. Kroemer, F. Madeo, Nucleocytosolic depletion of the energy metabolite acetyl-coenzyme A stimulates autophagy and prolongs lifespan. *Cell Metab.* **19**, 431–444 (2014).
18. D. N. Bagchi, A. M. Battenhouse, D. Park, V. R. Iyer, The histone variant H2A.Z in yeast is almost exclusively incorporated into the +1 nucleosome in the direction of transcription. *Nucleic Acids Res.* **48**, 157–170 (2020).
19. M. S. Kobor, S. Venkatasubrahmanyam, M. D. Meneghini, J. W. Gin, J. L. Jennings, A. J. Link, H. D. Madhani, J. Rine, A protein complex containing the conserved Swi2/Snf2-related ATPase Swr1p deposits histone variant H2A.Z into euchromatin. *PLoS Biol.* **2**, E131 (2004).
20. Y. Wan, R. A. Saleem, A. V. Ratushny, O. Roda, J. J. Smith, C. H. Lin, J. H. Chiang, J. D. Aitchison, Role of the histone variant H2A.Z/Htz1p in TBP recruitment, chromatin dynamics, and regulated expression of oleate-responsive genes. *Mol. Cell. Biol.* **29**, 2346–2358 (2009).
21. A. J. Morrison, X. Shen, Chromatin remodeling beyond transcription: The INO80 and SWR1 complexes. *Nat. Rev. Mol. Cell Biol.* **10**, 373–384 (2009).
22. N. J. Krogan, M. C. Keogh, N. Datta, C. Sawa, O. W. Ryan, H. Ding, R. A. Haw, J. Pootoolal, A. Tong, V. Canadien, D. P. Richards, X. Wu, A. Emili, T. R. Hughes, S. Buratowski, J. F. Greenblatt, A Snf2 family ATPase complex required for recruitment of the histone H2A variant Htz1. *Mol. Cell* **12**, 1565–1576 (2003).
23. G. Mizuguchi, X. Shen, J. Landry, W. H. Wu, S. Sen, C. Wu, ATP-driven exchange of histone H2A.Z variant catalyzed by SWR1 chromatin remodeling complex. *Science* **303**, 343–348 (2004).
24. X. Shen, G. Mizuguchi, A. Hamiche, C. Wu, A chromatin remodeling complex involved in transcription and DNA processing. *Nature* **406**, 541–544 (2000).
25. M. Papamichos-Chronakis, S. Watanabe, O. J. Rando, C. L. Peterson, Global regulation of H2A.Z localization by the INO80 chromatin-remodeling enzyme is essential for genome integrity. *Cell* **144**, 200–213 (2011).
26. S. Brahma, M. I. Udugama, J. Kim, A. Hada, S. K. Bhardwaj, S. G. Hailu, T. H. Lee, B. Bartholomew, INO80 exchanges H2A.Z for H2A by translocating on DNA proximal to histone dimers. *Nat. Commun.* **8**, 15616 (2017).
27. J. E. Babiary, J. E. Halley, J. Rine, Telomeric heterochromatin boundaries require NuA4-dependent acetylation of histone variant H2A.Z in *Saccharomyces cerevisiae*. *Genes Dev.* **20**, 700–710 (2006).
28. M. C. Keogh, T. A. Mennella, C. Sawa, S. Berthelet, N. J. Krogan, A. Wolek, V. Podolny, L. R. Carpenter, J. F. Greenblatt, K. Baetz, S. Buratowski, The *Saccharomyces cerevisiae* histone H2A variant Htz1 is acetylated by NuA4. *Genes Dev.* **20**, 660–665 (2006).
29. C. B. Millar, F. Xu, K. Zhang, M. Grunstein, Acetylation of H2AZ Lys 14 is associated with genome-wide gene activity in yeast. *Genes Dev.* **20**, 711–722 (2006).
30. P. Kemmeren, K. Sameith, L. A. L. van de Pasch, J. J. Benschop, T. L. Lenstra, T. Margaritis, E. O'Duibhir, E. Apweiler, S. van Wageningen, C. W. Ko, S. van Heesch, M. M. Kashani, G. Ampatzidis-Michailidis, M. O. Brok, N. A. C. H. Brabers, A. J. Miles, D. Bouwmeester, S. R. van Hooff, H. van Bakel, E. Sluiter, L. V. Bakker, B. Snel, P. Lijnzaad, D. van Leenen, M. J. A. Groot Koerkamp, F. C. P. Holstege, Large-scale genetic perturbations reveal regulatory networks and an abundance of gene-specific repressors. *Cell* **157**, 740–752 (2014).
31. C. Yi, M. Ma, L. Ran, J. Zheng, J. Tong, J. Zhu, C. Ma, Y. Sun, S. Zhang, W. Feng, L. Zhu, Y. Le, X. Gong, X. Yan, B. Hong, F. J. Jiang, Z. Xie, D. Miao, H. Deng, L. Yu, Function and molecular mechanism of acetylation in autophagy regulation. *Science* **336**, 474–477 (2012).
32. S. L. Beckwith, E. K. Schwartz, P. E. Garcia-Nieto, D. A. King, G. J. Gowans, K. M. Wong, T. L. Eckley, A. P. Paraschuk, E. L. Peltan, L. R. Lee, W. Yao, A. J. Morrison, The INO80 chromatin remodeler sustains metabolic stability by promoting TOR signaling and regulating histone acetylation. *PLoS Genet.* **14**, e1007216 (2018).
33. A. Ciechanover, Proteolysis: From the lysosome to ubiquitin and the proteasome. *Nat. Rev. Mol. Cell Biol.* **6**, 79–87 (2005).
34. H. Jeong, F. Then, T. J. Melia Jr., J. R. Mazzulli, L. Cui, J. N. Savas, C. Voisine, P. Paganetti, N. Tanese, A. C. Hart, A. Yamamoto, D. Krainc, Acetylation targets mutant huntingtin to autophagosomes for degradation. *Cell* **137**, 60–72 (2009).
35. M. Downey, J. R. Johnson, N. E. Davey, B. W. Newton, T. L. Johnson, S. Galaang, C. A. Seller, N. Krogan, D. P. Toczyski, Acetylome profiling reveals overlap in the regulation of diverse processes by sirtuins, gcn5, and esa1. *Mol. Cell. Proteomics* **14**, 162–176 (2015).
36. D. Coleman-Derr, D. Zilberman, Deposition of histone variant H2A.Z within gene bodies regulates responsive genes. *PLoS Genet.* **8**, e1002988 (2012).
37. L. T. Neves, S. Douglass, R. Spreafico, S. Venkataramanan, T. L. Kress, T. L. Johnson, The histone variant H2A.Z promotes efficient cotranscriptional splicing in *S. cerevisiae*. *Genes Dev.* **31**, 702–717 (2017).
38. T. L. Lenstra, J. J. Benschop, T. S. Kim, J. M. Schulze, N. A. C. H. Brabers, T. Margaritis, L. A. L. van de Pasch, S. A. A. C. van Heesch, M. O. Brok, M. J. A. Groot Koerkamp, C. W. Ko, D. van Leenen, K. Sameith, S. R. van Hooff, P. Lijnzaad, P. Kemmeren, T. Hentrich, M. S. Kobor, S. Buratowski, F. C. P. Holstege, The specificity and topology of chromatin interaction pathways in yeast. *Mol. Cell* **42**, 536–549 (2011).
39. W. Chen, X. Yu, Y. Wu, J. Tang, Q. Yu, X. Lv, Z. Zha, B. Hu, X. Li, J. Chen, L. Ma, J. L. Workman, S. Li, The SESAME complex regulates cell senescence through the generation of acetyl-CoA. *Nat. Metab.* **3**, 983–1000 (2021).
40. T. Noda, Y. Ohsumi, Tor, a phosphatidylinositol kinase homologue, controls autophagy in yeast. *J. Biol. Chem.* **273**, 3963–3966 (1998).
41. F. Reggiori, D. J. Klionsky, Autophagic processes in yeast: Mechanism, machinery and regulation. *Genetics* **194**, 341–361 (2013).
42. L. Pnueli, I. Edry, M. Cohen, Y. Kassir, Glucose and nitrogen regulate the switch from histone deacetylation to acetylation for expression of early meiosis-specific genes in budding yeast. *Mol. Cell. Biol.* **24**, 5197–5208 (2004).
43. J. R. Rohde, M. E. Cardenas, The tor pathway regulates gene expression by linking nutrient sensing to histone acetylation. *Mol. Cell. Biol.* **23**, 629–635 (2003).
44. T. Eisenberg, H. Knauer, A. Schauer, S. Büttner, C. Ruckstuhl, D. Carmona-Gutierrez, J. Ring, S. Schroeder, C. Magnes, L. Antonacci, H. Fussi, L. Deszcz, R. Hartl, E. Schraml, A. Cirillo, E. Megalou, D. Weiskopf, P. Laun, G. Heeren, M. Breitenbach, B. Grubeck-Loebenstein, E. Herker, B. Fahrenkrog, K. U. Fröhlich, F. Sinner, N. Tavernarakis, N. Minois, G. Kroemer, F. Madeo, Induction of autophagy by spermidine promotes longevity. *Nat. Cell Biol.* **11**, 1305–1314 (2009).
45. J. E. Brownell, C. D. Allis, Special HATs for special occasions: Linking histone acetylation to chromatin assembly and gene activation. *Curr. Opin. Genet. Dev.* **6**, 176–184 (1996).
46. J. Y. Kaimori, K. Maehara, Y. Hayashi-Takanaka, A. Harada, M. Fukuda, S. Yamamoto, N. Ichimaru, T. Umehara, S. Yokoyama, R. Matsuda, T. Ikura, K. Nagao, C. Obuse, N. Nozaki, S. Takahara, T. Takao, Y. Ohkawa, H. Kimura, Y. Isaka, Histone H4 lysine 20 acetylation is associated with gene repression in human cells. *Sci. Rep.* **6**, 24318 (2016).
47. S. Chen, Y. Jing, X. Kang, L. Yang, D. L. Wang, W. Zhang, L. Zhang, P. Chen, J. F. Chang, X. M. Yang, F. L. Sun, Histone H2B monoubiquitination is a critical epigenetic switch for the regulation of autophagy. *Nucleic Acids Res.* **45**, 1144–1158 (2017).
48. J. Füllgrabe, M. A. Lynch-Day, N. Heldring, W. Li, R. B. Struijk, Q. Ma, O. Hermanson, M. G. Rosenfeld, D. J. Klionsky, B. Joseph, The histone H4 lysine 16 acetyltransferase hMOF regulates the outcome of autophagy. *Nature* **500**, 468–471 (2013).
49. H.-J. R. Shin, H. Kim, S. Oh, J.-G. Lee, M. Kee, H.-J. Ko, M.-N. Kwon, K.-J. Won, S. H. Baek, AMPK-SKP2-CARM1 signalling cascade in transcriptional regulation of autophagy. *Nature* **534**, 553–557 (2016).
50. S. Zhang, X. Yu, Y. Zhang, X. Xue, Q. Yu, Z. Zha, M. Gogol, J. L. Workman, S. Li, Metabolic regulation of telomere silencing by SESAME complex-catalyzed H3T11 phosphorylation. *Nat. Commun.* **12**, 594 (2021).

51. B. Li, S. G. Pattenden, D. Lee, J. Gutiérrez, J. Chen, C. Seidel, J. Gerton, J. L. Workman, Preferential occupancy of histone variant H2A.Z at inactive promoters influences local histone modifications and chromatin remodeling. *Proc. Natl. Acad. Sci. U.S.A.* **102**, 18385–18390 (2005).
52. R. M. Raisner, P. D. Hartley, M. D. Meneghini, M. Z. Bao, C. L. Liu, S. L. Schreiber, O. J. Rando, H. D. Madhani, Histone variant H2A.Z marks the 5' ends of both active and inactive genes in euchromatin. *Cell* **123**, 233–248 (2005).
53. M. Adam, F. Robert, M. Laroche, L. Gaudreau, H2A.Z is required for global chromatin integrity and for recruitment of RNA polymerase II under specific conditions. *Mol. Cell. Biol.* **21**, 6270–6279 (2001).
54. C. M. Weber, S. Ramachandran, S. Henikoff, Nucleosomes are context-specific, H2A.Z-modulated barriers to RNA polymerase. *Mol. Cell* **53**, 819–830 (2014).
55. V. Subramanian, P. A. Fields, L. A. Boyer, H2A.Z: A molecular rheostat for transcriptional control. *F1000Prime Rep.* **7**, 01 (2015).
56. A. Auger et al., Eaf1 is the platform for NuA4 molecular assembly that evolutionarily links chromatin acetylation to ATP-dependent exchange of histone H2A variants. *Mol. Cell. Biol.* **28**, 2257–2270 (2008).
57. X. Cheng, A. Auger, M. Altaf, S. Drouin, E. Paquet, R. T. Utley, F. Robert, J. Côté, Eaf1 links the NuA4 histone acetyltransferase complex to Htz1 incorporation and regulation of purine biosynthesis. *Eukaryot. Cell* **14**, 535–544 (2015).
58. C. T. Werner, S. Mitra, J. A. Martin, A. F. Stewart, A. E. Lepack, A. Ramakrishnan, P. H. Gobira, Z. J. Wang, R. L. Neve, A. M. Gancarz, L. Shen, I. Maze, D. M. Dietz, Ubiquitin-proteasomal regulation of chromatin remodeler INO80 in the nucleus accumbens mediates persistent cocaine craving. *Sci. Adv.* **5**, eaay0351 (2019).
59. A. J. Morrison, Chromatin-remodeling links metabolic signaling to gene expression. *Mol. Metab.* **38**, 100973 (2020).
60. Q. Yu, X. Gong, Y. Tong, M. Wang, K. Duan, X. Zhang, F. Ge, X. Yu, S. Li, Phosphorylation of Jhd2 by the Ras-cAMP-PKA(Tpk2) pathway regulates histone modifications and autophagy. *Nat. Commun.* **13**, 5675 (2022).
61. J. Huang, W. Dai, D. Xiao, Q. Xiong, C. Liu, J. Hu, F. Ge, X. Yu, S. Li, Acetylation-dependent SAGA complex dimerization promotes nucleosome acetylation and gene transcription. *Nat. Struct. Mol. Biol.* **29**, 261–273 (2022).

**Acknowledgments:** We thank Li lab members for discussion of this project. **Funding:** This work was supported by funding from National Natural Science Foundation of China (31970578 to S.L. and 31872812 to X.Y.), Natural Science Foundation of Hubei Province (2021CFA013 to S.L. and 2019CFA077 to X.Y.). **Author contributions:** Conceptualization: S.L. and X.Y. Methodology: X.L., Q.Y., M.W., and F.G. Investigation: X.L., Q.M., F.H., D.X., and H.L. Visualization: X.L. Supervision: S.L. and X.Y. Writing—original draft: S.L. and X.Y. Writing—review and editing: S.L., X.Y., and X.L. **Competing interests:** The authors declare they have no competing interests.

**Data and materials availability:** All data needed to evaluate the conclusions in the paper are present in the paper and the Supplementary Materials. The ChIP-seq data for Rpd3 are available in the GEO database under the accession number GSE175868. The ChIP-seq data for H2A.Z used in this study are available in the GEO database under the accession number GSE116853. The RNA-seq data for *RPD3Δ* and *HTZ1Δ* mutants are available in the GEO database under the accession number GSE42527 and GSE97416, respectively. The RNA-seq data for *ATG3Δ* and *SWC7Δ* mutants are available in the GEO database under the accession number GSE42526. The RNA-seq data for *SWR1Δ*, *SWC3Δ*, and *ARP6Δ* mutants are available in the GEO database under the accession number GSE25909. The RNA-seq data for *BDF1Δ* mutant are available in the BioProject database under the accession number PRJNA612967. The mass spectrometry proteomics data have been deposited to the ProteomeXchange Consortium with the dataset identifier PXD035908 and PXD039052 (Ino80-FLAG) and PXD039051 (Rpd3-FLAG). The plasmids and strains can be provided by corresponding authors pending a completed material transfer agreement. Requests for the plasmids and strains should be submitted to: S.L. and X.Y.

Submitted 11 September 2022

Accepted 8 February 2023

Published 8 March 2023

10.1126/sciadv.ade8312